Special Issue: Unmanned Marine Systems

Regular Article

A domain-based and reactive COLAV method with a partially COLREGs-compliant domain for ASVs operating in confined waters

Emil Hjelseth Thyri and Morten Breivik

Centre for Autonomous Marine Operations and Systems (AMOS), Department of Engineering Cybernetics, Norwegian University of Science and Technology (NTNU), NO-7491 Trondheim, Norway

Abstract: This article presents a collision avoidance (COLAV) method for autonomous surface vessels operating in confined waters with other vessels, using a novel target ship (TS) domain. The domain is implemented as part of a reactive COLAV method pipeline through the use of control barrier functions (CBFs) to avoid domain violation. A geometric interpretation of a vessel-to-vessel encounter is used to classify the encounter type with respect to the COLREGs, and thereby which rules apply. Subsequently, a domain is assigned to the TS, where the domain parameters are rule-specific. In the domain design, the static environment is also considered, where an estimate for the available maneuverable space is calculated and applied when determining the size of each TS domain, in order to achieve a distance between vessels that is both safe and feasible for each encounter. Additionally, domains are assigned to static obstacles based on map data and lidar data. Once all domains for target ships and static obstacles are determined, CBFs are formulated based on the range to and velocity towards each domain. The set of CBFs are applied as inequality constraints in a quadratic program minimizing the vessel's thrust allocation error. The efficiency and completeness of the novel TS domain are demonstrated through an extensive simulation study. The COLAV method as a whole is demonstrated through both complex simulations with multiple maneuvering vessels, and full-scale experiments with a radar- and lidar-based target tracking system. The proposed COLAV method shows compliance with COLREGs section II.

Keywords: obstacle avoidance, motion planning, marine robotics

1. Introduction

A majority of the world's large urban areas are located around waterways, where the water bore a majority of the transport for centuries until the construction of roads and railways along with

Received: 22 June 2021; revised: 3 September 2021; accepted: 13 December 2021; published: 4 May 2022.

Correspondence: Emil Hjelseth Thyri, Centre for Autonomous Marine Operations and Systems (AMOS), Department of Engineering Cybernetics, Norwegian University of Science and Technology (NTNU), NO-7491 Trondheim, Norway., Email: emil.h.thyri@ntnu.no

Figure 1. The milliAmpere (blue in the middle), a prototype of an autonomous electric passenger ferry, during testing of multitarget tracking performance in a canal area in Trondheim in November, 2020. Two other vessels (upper right relative to milliAmpere) are used as target ships. Courtesy of Mikael Sætereid.

motorized land vehicles became the most efficient and cost-effective means of transportation. After this shift from water to land, many cities left the waterways underutilized. The recent development in technology enabling autonomous maritime operations has again made maritime transportation in urban waterways a competitive option, and several cities have taken an interest in renewed utilization of their waterways. There already exist several initiatives on this with the goal of increasing efficiency and flexibility while reducing the strain on existing infrastructure both in cargo transport (O'Dwyer, 2021; Blenkey, 2021) and passenger transport (Cairns, 2021). By applying an electric means of propulsion, benefits such as reduced cost, maintenance, and air and noise pollution can also be achieved.

While the potential benefits are many, so are the challenges. Maneuvering in urban waterways is no trivial task for either humans or machines due to a long list of considerations, such as traffic from commercial vessels and leisure craft, risk of grounding, global and local rules of maneuvering and navigation, traffic regulations, weather, and sea current. Not only do these aspects need to be considered in an autonomous planning, guidance, navigation, and vessel control system, but the information itself needs to be acquired through situational awareness systems consisting of sensors and algorithms for interpretation and comprehension to produce reliable information that can be applied by the planners.

Due to the task complexity of autonomous maritime operations, and in particular the collision avoidance (COLAV) objective, autonomous guidance navigation and control (GNC) systems are often composed of multiple layers of planners in what is referred to as a hybrid structure. In such structures, the effectiveness of several planners can be exploited by distributing the planning responsibility to match each planner's capacity. An illustration of a three-layered structure is displayed in Figure 2 along with several examples of situational awareness modules that one or more of the planners might apply.

The high-level COLAV module performs long-term or global path or trajectory planning with respect to, e.g., map data from electronic nautical charts (ENCs), weather and ocean current data, departure and arrival time, and traffic regulations such as allocated fairways or traffic separation

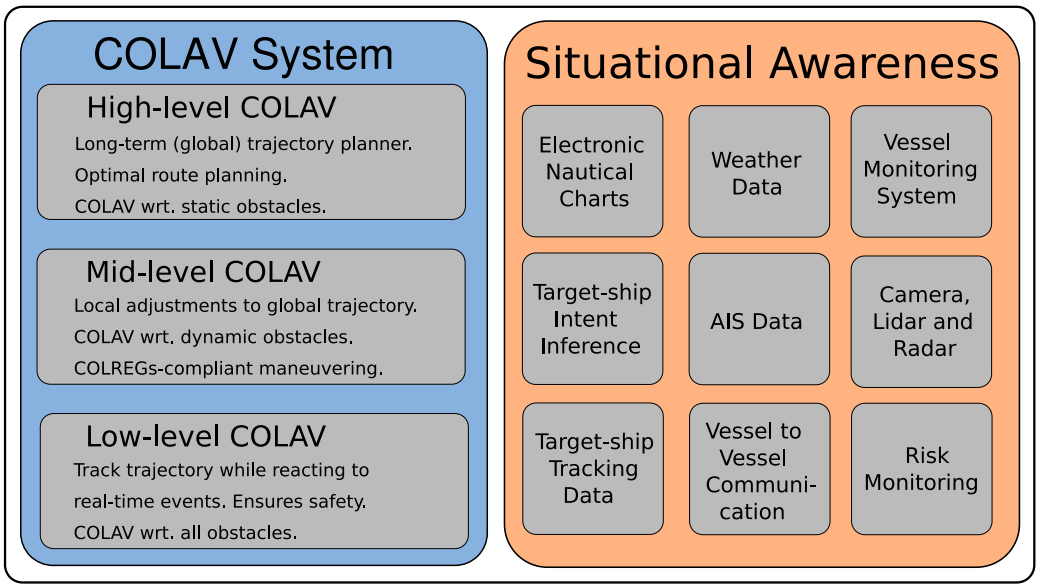

Figure 2. Example of a hybrid COLAV structure, where each of the modules in the COLAV system might apply one or more of the situational awareness modules.

schemes. The high-level planner can run once at the start of a transit or periodically with a long period between each iteration.

The midlevel COLAV module considers COLREGs in vessel-to-vessel (V2V) encounters, and it makes adjustments to the nominal path or trajectory from the high-level planner to comply with the relevant regulations. The planning can be performed based on target data from either an automatic identification system (AIS) or a target tracking system based on exteroceptive sensors. The planning horizon of the midlevel COLAV can be from several seconds to several minutes, with a planning period suitable for the rate of change of the relevant features in the environment.

The low-level COLAV module should have a short planning horizon relative to the dynamics of the operational environment, and for several applications it can be purely reactive, where it reacts to current states without deliberation. The task of the low-level planner is to resolve immediate situations in a safe manner. For autonomous surface vessels (ASVs), that means mainly avoiding collision with all obstacles, both static and dynamic, while adhering to the relevant protocol.

The benefit of a hybrid approach is demonstrated in (Loe, 2008; Svec et al., 2013; Eriksen et al., 2020), where the latter article is an excellent example of a three-layer structure where the top layer performs energy-optimized path planning, the midlevel handles long-term COLAV regarding static and dynamic obstacles while enforcing parts of the relevant protocol, and the lowest level handles reactive COLAV and emergency situations. A noteworthy feature in the hybrid structure proposed in (Eriksen et al., 2020) is that the midlevel algorithm disregards dynamic obstacles with a distance at closest point of approach (DCPA) and time at closest point of approach (TCPA) below some threshold value, since its run period and horizon make it unsuited for considering those obstacles in the planner. This leaves the low-level COLAV algorithm to resolve the immediate situations. This is particularly relevant in highly dynamic environments where the obstacle behavior is changing at periods equal to or smaller than the available planning periods, and the plan from a higher level planner might be outdated before a new and updated plan is produced. This applies in particular in urban maritime environments, where the field of view can be restricted by both static and dynamic obstacles, and the variety of vessels and vessel operators make the traffic unpredictable. The lack of AIS equipment on smaller vessels restricts the detection range to the field of view of

the vessel's exteroceptive sensor system, often composed of radar, lidar, and camera combinations, which reduces the effectiveness of the long-term planners. A complete and safe low-level COLAV is therefore paramount for operation in such environments. A suitable low-level COLAV module can ensure the baseline safety of the whole hybrid collision-avoidance structure by resolving close-range encounters in a satisfactory and safe manner every time.

The contribution of this paper is a reactive COLAV system for ASVs, suitable for the lowest level in a hybrid structure like the one in Figure 2. The method is designed for operation in confined waters where traffic is unpredictable and detection is limited by the field of view. However, it also performs well in open waters where the presence of leisure vessels makes predictions on future TS behavior uncertain. The method handles static and dynamic obstacles, where considerations on relevant parts of the COLREGs are included, in particular compliance with Rules 13–15 and partial fulfillment of Rules 8 and 17, regarding vessels in sight of one another. The main novelty of this work is the target ship (TS) domain design, where a rule-based approach is applied to assign a domain to each of the tracked dynamic obstacles, and the COLREGs considerations are encoded in the qualities of the domain. Additionally, a metric for the available maneuverable space is included in the dimensioning of the TS domain to ensure that the DCPA is adjusted to suit each individual encounter. The domain design is simple and intuitive, and is encoded by a small set of parameters for each of the relevant rules in the COLREGs. Additionally, similar domains are assigned to relevant static obstacles. Once a domain is assigned, a safe set is defined as a function of the range to, and relative velocity towards, each TS domain and static obstacle domain. Lastly, a control barrier function (CBF) is formulated for each domain. The CBFs are applied as inequality constraints in an optimization problem that minimizes the error between a virtual control from the trajectory tracking control system and a virtual control that ensures forward invariance of the safe set. The proposed TS domain is demonstrated through an extensive set of simulations, while the method as a whole is demonstrated through both simulations and full-scale experiments in a relevant environment, with a radar- and lidar-based target tracking system, and a combination of lidar and map data for COLAV with static obstacles.

The remainder of this paper is structured as follows: Section 2 provides a review of relevant previous work. Section 3 presents a theory on COLREGs and CBFs. In Section 4, we present the considerations that go into the TS domain design, and we define the domain. Section 5 contains a brief description of how the domain for static obstacles is constructed. In Section 6, we formulate the CBFs that ensure that the domains for static and dynamic obstacles are not violated. Sections 7 and 8 present the simulation and experimental results, respectively, before Section 9 finally concludes the paper.

2. Previous work

This section reviews previous work on COLAV for ASVs. We focus the review in particular on work directed towards confined waters operations with high traffic, and work with an experimental contribution. For a more substantial review of COLAV algorithms, the reader is advised to consult the recent survey papers on the field in (Vagale et al., 2021b) for a review of the field of path planning and COLAV for ASVs, (Vagale et al., 2021a) for a comparative study of existing COLAV algorithms, and (Huang et al., 2020) for a structured breakdown of the techniques that go into maritime COLAV, and a discussion of state-of-the-art approaches to each subproblem of maritime COLAV.

In (Benjamin et al., 2006), perhaps the first demonstration of an autonomous partial protocol compliant COLAV system tested on a marine platform is presented. The proposed method calculates a utility for a set of candidate legs for an ASV trajectory, parametrized by course, speed, and duration from the current state, and realizes the highest utility maneuver. The base utility for each leg is a measure of its contribution to progress towards the mission goal position. Inclusion of COLAV is encoded by a reduction in utility based on the estimated closest point of approach (CPA) for that leg. COLREGs considerations for Rules 14–16 as well as parts of Rule 8 are included by further reduction

in utility for nonreadily apparent maneuvers, maneuvers that pass in front of crossing vessels and maneuvers that pass starboard to starboard in head-on encounters. The method is demonstrated through experiments with two kayak-based ASVs, with a shared GPS position for target tracking. The method is only tested in V2V encounters, and does not consider static obstacles.

In (Schuster et al., 2014), a method for target tracking is presented in which data from a low-cost radar are applied. The method is intended for smaller vessels, and it considers a use-case with leisure vessels maneuvering on an inland lake. In the paper, a grid-based graph-search method is applied for finding the shortest-path collision-free trajectory at constant speed. The method applies the TS domain proposed in (Goodwin, 1975), where three circle sectors of varying radial extension are assigned to the TS's starboard forward side, port forward side, and aft of the TS, with the longest radial extension on the starboard forward side, and the shortest radial extension at the aft. The domain makes the trajectory planner favor maneuvering to pass port to port in head-on encounters, and behind the TS in crossing encounters. The paper presents a full-scale experiment, where two leisure vessels of approximately 6 m in length meet in a crossing encounter. However, since no classification of an encounter is made, and the TS domain is the same for all encounters, the method has no distinction between stand-on or give-way encounters.

In (Kuwata et al., 2014), a version of the velocity obstacle (VO) algorithm assigns a domain to the TS that includes both the extension of the ownship (OS), which is the vessel that is controlled, and the TS. The method also accounts for uncertainty in the velocity estimate of the TS when computing the velocity obstacle. The authors have encoded Rules 14–15 of the COLREGs directly into the velocity space by considering at what side of the TS the OS should pass. Detected hazards with a speed below a certain threshold are treated as stationary hazards where no rules apply. The method is demonstrated through full-scale experiments in scenarios with up to three target ships, where a radar and stereo cameras are applied as perceptive sensors for target tracking.

Further protocol considerations are included in the VO algorithm in (Woerner, 2016) by designing explicit metrics for protocol compliance with each of the relevant rules, which are used in cost calculations for each velocity pair. The proposed method shows good performance and protocol compliance with the relevant COLREGs parts. The algorithm is demonstrated through extensive simulation, where a proposed automatic evaluation scheme shows a clear distinction between the algorithm with and without consideration of COLREGs. The work also includes an extensive experimental effort with up to five vessels in multiagent scenarios. In the experiments, the GPS position of each vessel was transmitted to all vessels for target tracking.

In (Eriksen et al., 2019; Eriksen and Breivik, 2019), a graph-based COLAV algorithm for high-speed ASVs, named the branching-course model predictive control algorithm, which considers both static and dynamic obstacles, is presented. The algorithm simulates combinations of a finite set of course and speed change maneuvers in succession to get a set of trajectory candidates from the current position. The proposed method handles protocol compliance by assigning cost to each trajectory candidate based on its intersection with a TS domain, where the domain is elliptical-like with increasing cost towards the center, and the TS shifted towards the port and back side of the domain to favor maneuvers that pass behind or on the port side of the TS. This motivates trajectories that comply with Rules 13–15. The algorithm is demonstrated through full-scale experiments with a high-speed ASV and one TS, where a radar-based target-tracking system is applied. An effort is also made to make the algorithm robust to noise from the target tracking system by applying a cost to transitioning from the current trajectory, hence reducing the risk of alternating between several trajectories.

In (Shah et al., 2016), explicit steps are taken towards handling the problem of high traffic, where the authors present a lattice-based risk and contingency-aware planner for congested waters with high traffic. In the approach, the common assumptions of constant TS behavior are mitigated by predicting protocol-compliant trajectories for each TS, and applying them in the search for feasible trajectories. The method is demonstrated through simulations with up to three target ships, and compared to a variation of the VO described in (Kuwata et al., 2014), where it achieves a reduced number of collisions.

The mentioned methods all consider COLAV with respect to both static and moving obstacles with some regard to COLREGs. However, very few of the existing methods consider explicitly COLAV in confined waters, where the presence of static obstacles needs to be taken into account when considering maneuvers with respect to (w.r.t.) dynamic obstacles. In particular, acceptable distance at CPA, which will vary greatly with the available maneuverable space, needs to be taken into account in the domain design when applying strict TS domains to ensure feasibility in confined spaces, and safety in more open waters.

3. Background theory

This section introduces background theory for the reactive COLAV method that will be presented in the next sections. First an introduction to the relevant paragraphs in the COLREGs is given, and subsequently we introduce the vessel model that we consider. Lastly, we provide background theory on CBFs and how they can be applied effortlessly as inequality constraints to a quadratic optimization problem.

3.1. COLREGs—The rules of the road

The COLREGs are the result of a convention developed over several decades to prevent collision between two or more vessels at sea, which in 1972 was revised and given its current name. The convention is continuously tested and revised to be unambiguous as new technology and maritime applications occur. The COLREGs apply to all vessels upon the high seas and all waters connected to the high seas and navigable by seagoing vessels.

The convention has four main parts: Part A—General, Part B—Steering and Sailing, Part C—Lights and Shapes, and Part D—Sound and Light signals. In the work presented here, we focus on maneuvering of an ASV in the presence of other vessels, and hence it is the rules in Part B, regarding vessels in sight of one another, that are most relevant. Here follows a short description of the rules we consider, while Figure 3 provides illustrations of situations where rules apply, as seen from the OS in blue in a V2V encounter with a TS in red. A more comprehensive description of the rules can be found in (Cockcroft and Lameijer, 2012).

- **Rule 8** *Any action to avoid collision shall, if circumstances of the case admit, be positive, made in ample time, and with due regard to good seamanship.*
- **Rule 13** *Any vessel overtaking another vessel shall keep out of the way of the vessel being overtaken. A vessel approaching another vessel from a direction of more than* 22.5 deg *abaft*

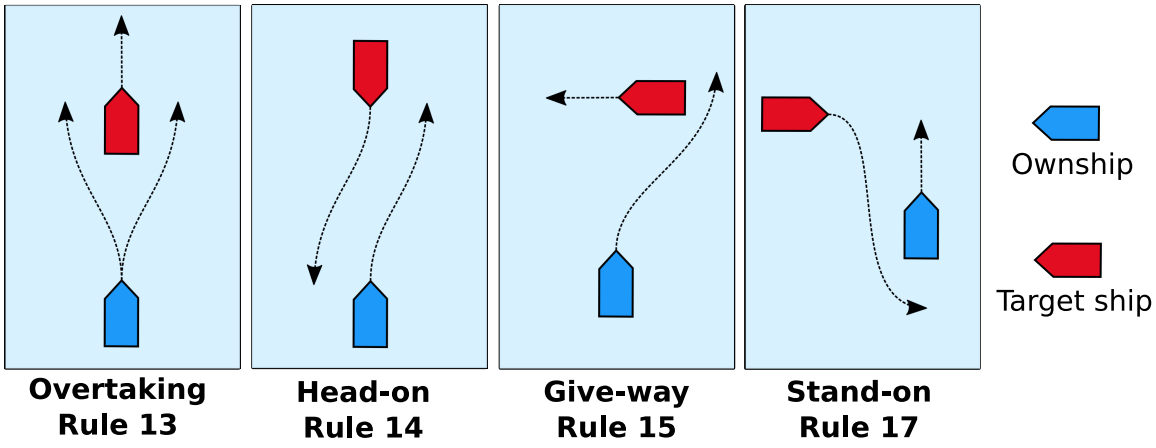

Figure 3. Illustration of COLREGs rules 13–15 and 17, as seen from the OS in blue.

her beam is an overtaking vessel. Any subsequent alternation of bearing between the two vessels shall not relieve the overtaking vessel of the duty of keeping clear of the overtaken vessel until she is finally past and clear.

- **Rule 14** *When two power-driven vessels are meeting on reciprocal or nearly reciprocal courses so as to involve risk of collision, each shall alter her course to starboard so that each shall pass on the port side of the other.*
- **Rule 15** *When two power-driven vessels are crossing so as to involve risk of collision, the vessel that has the other on her own starboard side shall keep out of the way and shall, if the circumstances of the case admit, avoid crossing ahead of the other vessel.*
- **Rule 16** *Every vessel that is directed to keep out of the way of another vessel shall, so far as possible, take early and substantial action to keep well clear.*
- **Rule 17** *Where one of two vessels is to keep out of the way, the other shall keep her course and speed. The latter vessel may take action to prevent collision if it is apparent that the vessel required to keep out of the way is not taking appropriate action.*

3.2. Control barrier functions

CBFs have emerged in recent years as the safety equivalent to what control Lyapunov functions (CLFs) are for stability (Ames et al., 2019). CBFs are used for set-based control to ensure forward invariance for some set $\mathcal{C}$. The set $\mathcal{C}$ can then be designed for the operational task at hand to be a safe set.

In this paper, we consider nonlinear control affine systems on the form

$$\dot{\boldsymbol{x}} = \boldsymbol{f}(\boldsymbol{x}) + \boldsymbol{g}(\boldsymbol{x})\boldsymbol{u}, \quad \boldsymbol{x}(0) = \boldsymbol{x}_0, \tag{1}$$

where $\boldsymbol{f} : \mathbb{R}^n \to \mathbb{R}^n$ and $\boldsymbol{g} : \mathbb{R}^n \to \mathbb{R}^m$ are locally Lipschitz, $\boldsymbol{x} \in D \in \mathbb{R}^n$ contains the states of the system, and $\boldsymbol{u} \in U \in \mathbb{R}^m$ is the control input. Such systems describe a variety of field robotic systems in air, on land, and at sea, and they have the same form as the three degrees of freedom (3DOF) model in (Fossen, 2011), commonly used for ASVs. Further, we assume a set $\mathcal{C}$ that is safe regarding the system task. This set is said to be forward invariant with respect to (1) if for a given solution to (1), $\boldsymbol{x} : [0, t_1] \to \mathbb{R}^n$,

$$\boldsymbol{x}(0) \in \mathcal{C} \implies \boldsymbol{x}(t) \in \mathcal{C}, \quad \forall t \in [0, t_1]. \tag{2}$$

A CBF is a continuously differentiable function $h\colon \mathbb{R}^n \to \mathbb{R}$, where the safe set $\mathcal{C}$ is defined as a super-zero-level set to $h(\boldsymbol{x})$, that is,

$$\begin{aligned} \mathcal{C} &= \{\boldsymbol{x} \in \mathbb{R}^n : h(\boldsymbol{x}) \geq 0\}, \\ \partial\mathcal{C} &= \{\boldsymbol{x} \in \mathbb{R}^n : h(\boldsymbol{x}) = 0\}, \\ \mathrm{Int}(\mathcal{C}) &= \{\boldsymbol{x} \in \mathbb{R}^n : h(\boldsymbol{x}) > 0\}, \end{aligned} \tag{3}$$

where $\mathrm{Int}(\mathcal{C})$ is the interior of $\mathcal{C}$. Ensuring invariance of $\mathcal{C}$ implies that $h(\boldsymbol{x}) \geq 0$ along the trajectories of (1). Positivity of $h(\boldsymbol{x})$ can be shown if

$$\dot{h}(\boldsymbol{x}(t)) = \frac{\partial h}{\partial \boldsymbol{x}} \left(f(\boldsymbol{x}) + g(\boldsymbol{x})\boldsymbol{u}(\boldsymbol{x})\right) \geq -\gamma\left(h(\boldsymbol{x}(t))\right) \tag{4}$$

for some extended class-κ function $\gamma : \mathbb{R} \to \mathbb{R}$. If there exists a continuous function $\boldsymbol{u} : \mathbb{R}^n \to \mathbb{R}^m$ such that (4) is satisfied, then $h(\boldsymbol{x})$ is a valid CBF for the system in (1).

CBFs on the form of (4) can be applied as inequality constraints to an optimization-based control allocation such as

$$\boldsymbol{u}^* = \min_{\boldsymbol{u}} \frac{1}{2} ||\boldsymbol{u} - \boldsymbol{k}(\boldsymbol{x})^2|| \tag{5}$$

minimizing the allocation error between a nominal control input $\boldsymbol{k}(\boldsymbol{x})$ and a control input that adheres to the constraints. The nominal control input $\boldsymbol{k}(\boldsymbol{x})$ can be provided by an arbitrary controller that is suitable for the control objective.

4. Target ship domain design

This section presents the main contribution of this work, namely the TS domain design. The proposed TS domain is rule-based, in that the parameters that define the domain are chosen from a set based on a geometric classification of the encounters that determine which of the Rules 13–15 or 17 apply. We introduce the method for encounter classification in Section 4.1. Subsequently, in Section 4.2, we propose a measure for the available maneuverable space for the OS when passing a TS, which is used in determining the extension of the TS domain. In Section 4.3, the criteria for passing with the TS on the port or starboard side are formulated. Lastly, in Section 4.4, the TS domain is formulated.

4.1. Encounter classification

In this paper, encounter classification means the process of determining the encounter type from the viewpoint of the OS in a V2V encounter, and thereby which of the COLREGs rules should be followed by the OS. There are several methods for such classification, most of which deem the OS to be in one of the following encounters, where the corresponding rules apply.

- Overtaking (OT): **Rule 13**.
- Head-on (HO): **Rule 14**.
- Give-way (GW): **Rule 15**.
- Stand-on (SO): **Rule 17**.
- Safe (SF): No rules apply.

(Woerner, 2016) describes an algorithm for encounter classification based on the relative bearing of the OS from the TS as well as the relative bearing of the TS from the OS, where numerical values from the COLREGs are applied as entry criteria. In (Tam and Bucknall, 2010) another method for classification based on the encounter geometry is described. The method is a two-step process. In the first step, the relative bearing sector (RBS)[1] is determined based on the relative bearing of the TS from the OS,

$$\varphi = \text{atan2}((E_{TS} - E), (N_{TS} - N)) - \chi, \tag{6}$$

and a set of sector angles that divide a circle into six sectors, where the OS is at the center of the circle. Here, χ is the course of the OS, while N and E, and N_{TS} and E_{TS}, are the north and east position of the OS and TS, respectively. The RBS is chosen based on which sector φ lies within. In the second step, the course of the TS relative to the OS,

$$\chi_{rel} = \chi_{TS} - \chi, \tag{7}$$

is applied, along with the same set of sector angles, to determine the situation sector (SS),[2] and hence the encounter classification.

This method is intuitive and easy to follow, as it has a visual geometric interpretation. In (Eriksen et al., 2020), this classification method is augmented by the use of the relative velocity between the OS and the TS to deem some OT, GW, and SO encounters safe when the range between the vessels is increasing. In addition, a state machine is applied to hold any classification other than SF until the

[1] The RBS are denoted R1 to R6 in (Tam and Bucknall, 2010)
[2] The SS are denoted TSR1 to TSR6 in (Tam and Bucknall, 2010)

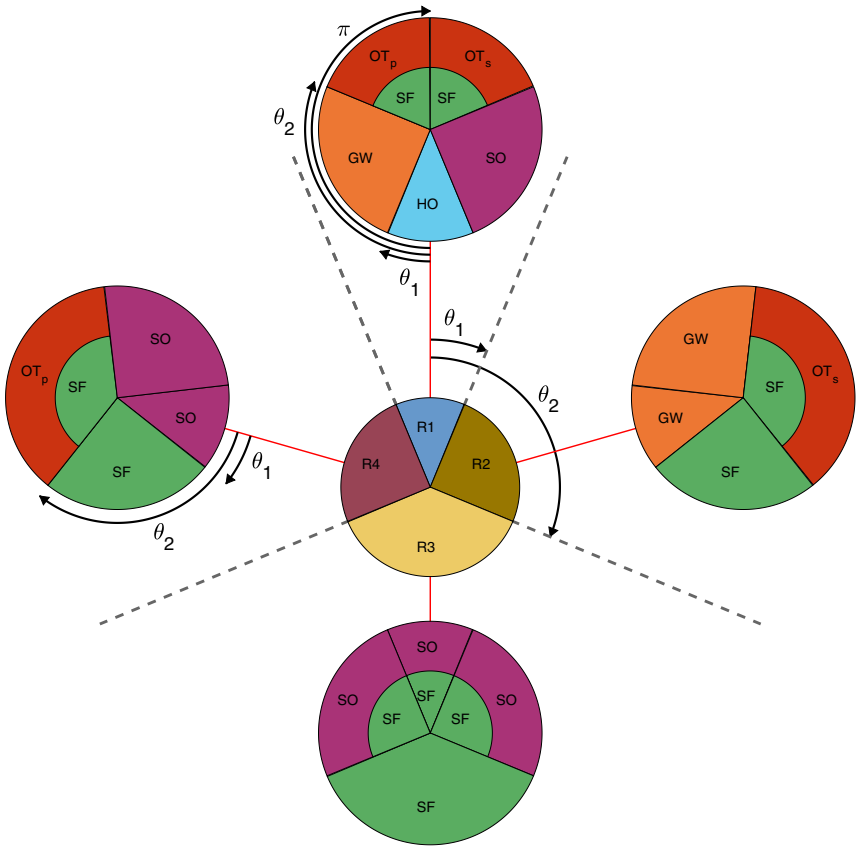

Figure 4. Graphic representation of the classification algorithm, where the position of the OS is at the center of the middle circle. In situation sectors with two encounter classifications, the outer one is chosen when the involved vessels have a closing range, while the inner one is chosen for increasing range.

encounter is once again classified as safe. This ensures that the latter part of **Rule 13** is overheld, which states that a give-way vessel needs to be past and clear to be relieved of its give-way duty. In (Thyri et al., 2020a), a further addition to the classification is introduced, with a distinction made as to whether an overtaking should be conducted with the TS on the port or starboard side, denoted OT_s and OT_p, respectively. The distinction is based on χ_{rel}, choosing OT_p for $\chi_{rel} \geq 0$ and OT_s for $\chi_{rel} < 0$, and facilitates crossing behind the TS in close-quarter overtaking encounters.

However, this classification method has a flaw that results in wrongful classifications in several V2V encounter geometries. The error originates from the use of χ_{rel} in the second step of the classification, while applying the same set of sector angles as was used in the first step. The relative heading between the vessels relates somewhat, but not accurately, to the criteria for encounter classification in COLREGs, as it is the visual reading of the lights of the vessels by night, or "the corresponding aspect of the other vessel" by day, that is the wording of the protocol.

In this paper, therefore, we apply a classification method that is very similar to the method presented in (Tam and Bucknall, 2010), and we have improved on the shortcomings so that the classification is correct, with respect to COLREGs, for all V2V geometries. A graphical representation of the method is given in Figure 4. In the first step, the RBS is determined based on φ and the sector angles $[-\theta_2, -\theta_1, \theta_1, \theta_2]$ in the same way as for the original method, however with a reduced set of sector angles. This will put the TS in one of the four RBS: R1, R2, R3, or

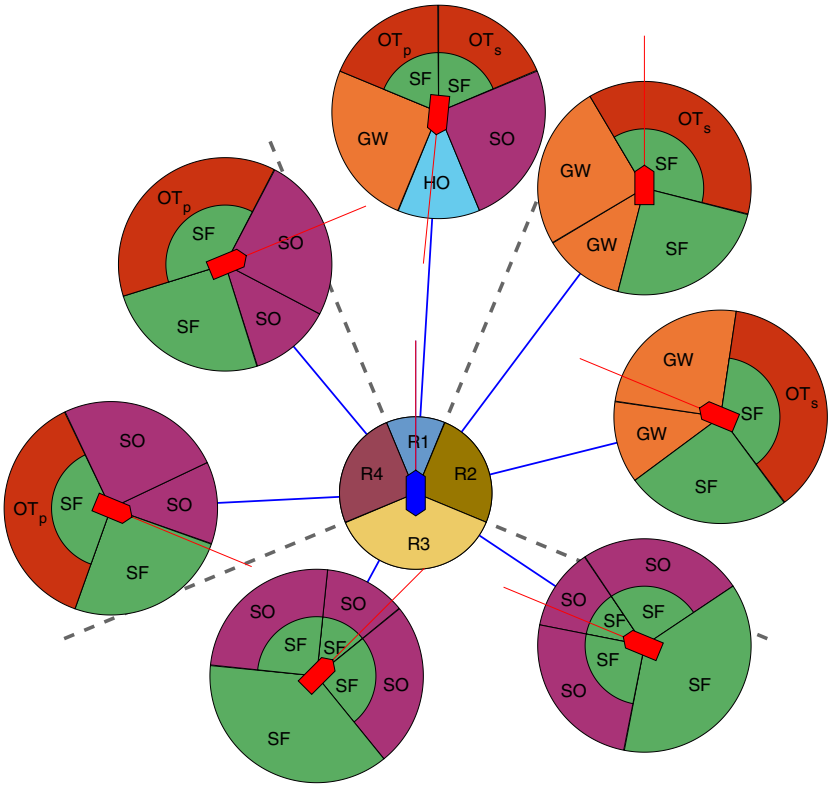

Figure 5. Classification examples for an arbitrary set of target ships (red), and the blue OS. Classification is made by selecting the encounter type of the sector within which the TS course vector lies.

R4. Subsequently, the SS is determined by χ_{rel}, with a set of rotated sector angles $[-\theta_2^{'}, -\theta_1^{'}, \theta_1^{'}, \theta_2^{'}]$, where $\theta_1^{'} = \theta_1 - \varphi_{TS}$ and $\theta_2^{'} = \theta_2 - \varphi_{TS}$, and

$$\varphi_{TS} = \text{atan2}((E - E_{_{TS}}), (N - N_{_{TS}})) \tag{8}$$

is the bearing of the OS from the TS. Figure 5 shows how the graphical geometric representation of the method can be used to classify an encounter. In the figure, the OS is at the center, and each TS has its own shifted situation sector circle. The classification is done visually by choosing the sector in which the course vector of the TS lies. We also include a state machine as proposed in (Eriksen et al., 2020), where a classification is held static if the range between the vessels is below some threshold.

4.2. Maneuverable space

Close quarters, risk of collision, ample time, and close proximity are all relative terms. Yet they are applied in the COLREGs formulation of how and when vessels in sight of one another are obliged to maneuver. As one may imagine, quantitative interpretation of these terms is very much dependent on the individual situation, and in particular the surroundings. For two vessels moving in confined waters, e.g., a harbor, canal, or an area where the vessel draft is restricting maneuverability, passing at 30, 20, or even 10 m can be considered acceptable, while doing this in open waters would be considered misconduct, and in violation of the practice of good seamanship and the COLREGs. For vessels moving in confined waters, the accepted DCPA is therefore highly dependent on the

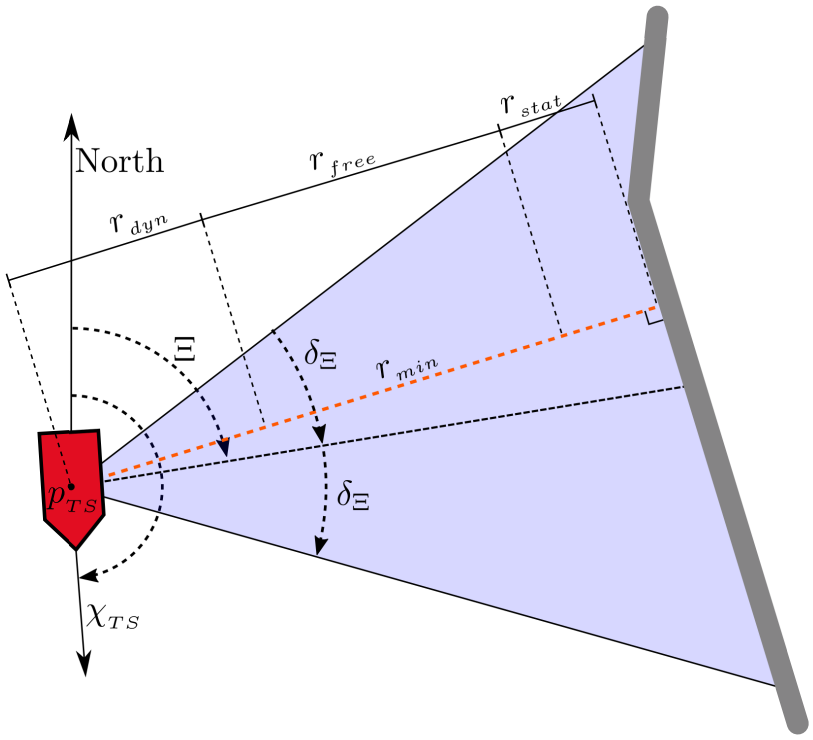

Figure 6. Illustration of a pass sector (blue) for a TS located at p_{TS} with an arbitrary static obstacle illustrated by the thick grey line. The minimum free range of the pass sector, $r_{min} \geq 0$, is indicated by the dashed red line. The distances $r_{dyn} \geq 0$ and $r_{stat} \geq 0$ are the minimum ranges that are considered not to be a collision with a dynamic obstacle or a static obstacle, respectively.

available maneuverable space, and it is paramount that this should be considered when determining the shortest allowable DCPA in an encounter.

We propose the use of an adaptive measure, r_{free}, for the available maneuverable space for an encounter, which we later will use in determining the size l of the TS domain. When calculating r_{free} for a V2V encounter, first the pass sector, i.e., the sector around the TS where the OS should pass, is determined. Subsequently, the shortest distance from the TS to any static obstacle in the pass sector is found. The pass sector is given by the encounter classification. We denote the pass sector by two angles, $\Xi \in [-\pi, \pi]$ and $\delta_\Xi \in [-\pi, \pi]$, where the pass sector is the sector swiped by a line starting in p_{TS} and swiping the sector $[\Xi - \delta_\Xi, \Xi + \delta_\Xi]$. Figure 6 shows the pass sector in blue for a TS located at p_{TS}. The minimum range to a static obstacle within the pass sector, r_{min}, is indicated by the red dashed line. The free range is given by

$$r_{free} = r_{min} - r_{dyn} - r_{stat}, \tag{9}$$

where

$$r_{dyn} = \frac{1}{2}(l_{OS} + l_{TS}) + \delta_{dyn} \tag{10}$$

is the minimum DCPA to a dynamic obstacle at which no collision will occur, and

$$r_{stat} = \frac{1}{2} l_{OS} + \delta_{stat} \tag{11}$$

is the minimum distance to a static obstacle at which no collision will occur. Here, l_{OS} and l_{TS} are the lengths of the OS and TS, respectively. The distances δ_{dyn} and δ_{stat} are additional tolerances to dynamic and static obstacles, respectively. The tolerance should account for uncertainties in map

data, target tracking, and navigation. Calculating r_{free} requires *a priori* knowledge of the area in the form of map data, which is a fair assumption to have for most ASV operations, in which map data would also be required for long-term path or trajectory planning. Such data are often readily available from online map services, as is the case for the map data used in the experiments in this paper[3] (Kartverket, 2020).

4.3. Passing on port or starboard

In a V2V encounter where risk of collision exists, at least one vessel is obliged by the COLREGs to take action to avoid collision. The maneuvering guidelines are largely focused on what is the preferred side of the OS that the TS should be on when passing. For most encounters, if the circumstances allow, it is the port side, except for overtaking encounters, where the maneuvering choice is dependent on other factors. At the same time, some close quarter encounters can be resolved by passing with the TS on the starboard side with little or no maneuvering effort, where passing with the TS on the port side would require extensive maneuvering effort, either due to the encounter geometry or the velocity of the vessels. We therefore propose a method to determine on which side to pass the TS that considers these factors through the encounter classification, the geometry of the encounter, and the relative velocity vector between the two vessels,

$$\boldsymbol{U}_{rel} = \boldsymbol{U}_{TS} - \boldsymbol{U}_{OS}, \tag{12}$$

where $\boldsymbol{U}_{OS} \in \mathbb{R}^2$ and $\boldsymbol{U}_{TS} \in \mathbb{R}^2$ are the northeast velocity vectors of the OS and TS, respectively. The distinction is made based on the bearing of the OS from the TS relative to the port-starboard split angle

$$\alpha_s = \alpha_{U\_rel} + \alpha_{\delta\_s}, \tag{13}$$

where

$$\alpha_{U\_rel} = \text{atan2}(U_{E\_rel}, U_{N\_rel}) \tag{14}$$

is the angle of the relative velocity vector relative to north, with U_{N_rel} and U_{E_rel} as the north and east components of $\boldsymbol{U}_{rel}$, respectively. The bias $\alpha_{\delta\_s} \in [-\pi/2, \pi/2]$ is a classification-specific offset that will facilitate protocol-compliant maneuvers. Maneuvering to port to pass with the TS on the OS starboard side is preferred if $\varphi_{TS} > \alpha_s$, and maneuvering to starboard to pass with the TS on the OS port side is preferred if $\varphi_{TS} \leq \alpha_s$.

Since the α_{U_rel} is undefined when the relative velocity is zero, and is prone to noise from both target tracking and navigation when the relative velocity is low, a weighted average between α_{U_rel} and φ_{TS} is applied when $||U_{rel}|| < U_{lim}$. That is,

$$\alpha_s = \begin{cases} \alpha_{U\_rel} + \alpha_{\delta\_s} & \text{if } ||U_{rel}|| \geq U_{lim}, \\ \frac{||U_{rel}||}{U_{lim}} \alpha_{U\_rel} + (1 - \frac{||U_{rel}||}{U_{lim}}) \varphi_{TS} + \alpha_{\delta\_s} & \text{if } ||U_{rel}|| < U_{lim}. \end{cases} \tag{15}$$

In addition to the broad considerations in this distinction, the α_s angle also reduces the chance of oscillating behavior that can result from noise or uncertainty in the position and velocity estimates for the OS and TS when the φ_{TS} is close to α_s, since the absolute difference $|\alpha_s - \varphi_{TS}|$ will increase once a maneuver is initiated due to the resulting changes in the relative velocity vector, effectively increasing the commitment to the maneuver. The same is true for maneuvers by the TS.

4.4. Target ship domain definition

Once the encounter is classified, the available maneuverable space is estimated, and at what side of the TS the OS should pass is determined, a domain can finally be assigned to the TS. The TS

[3] Adjustments were made to the original map data to better represent floating docks and docked vessels.

domain that we propose is a straight line dividing the northeast plane into two halves. The half plane containing the TS is the TS domain. The domain is defined by the position of the TS, and two variables:

- $l \geq r_{dyn}$ is the shortest distance from the TS to the line defining the domain,
- $\alpha \in [-\pi, \pi]$ is the angle of the normal vector to the domain, pointing away from the TS.

The TS domain is considered as an unsafe set, denoted $\mathcal{C}_{u\_dyn\_i}$ for TS i, where $i \in [1, N_{TS}]$, and N_{TS} is the number of tracked target ships. We will later use $\mathcal{C}_{u\_dyn\_i}$ to define the safe set $\mathcal{C}$. In the choice of l, the available maneuverable space is considered, where we choose

$$l = \begin{cases} r_{dyn} & \text{if } r_{free} <= 0, \\ r_{dyn} + k_l r_{free} & \text{if } r_{free} < r_{free\_max}, \\ r_{dyn} + k_l r_{free\_max} & \text{if } r_{free} >= r_{free\_max}, \end{cases} \tag{16}$$

where $k_l \in [0, 1]$ is a design parameter that splits the free maneuverable space between the TS and a potential static obstacle. The angle of the normal vector is defined as

$$\alpha := \alpha_s + \alpha_D, \tag{17}$$

where

$$\alpha_D = \begin{cases} \varphi_{TS} - \alpha_s + \alpha_d & \text{if } \varphi_{TS} > \alpha_s, \\ \varphi_{TS} - \alpha_s - \alpha_d & \text{otherwise.} \end{cases} \tag{18}$$

Here $\alpha_d \in (-\pi/2, \pi/2)$ is the deflection angle, a classification-specific parameter. This angle is used to alter the deflection of the OS on the TS domain to both avoid stagnation when the OS is approaching the TS at a near right angle, and to facilitate passing the TS with a geometry that complies with the relevant rule. The reason we go through α_D when calculating α is that saturation is applied to this variable so that $\alpha_D \in [\alpha_{D\_min}, \alpha_{D\_max}]$. The rationale behind this saturation will be discussed shortly.

Lastly, we define two points on the TS domain, namely $\boldsymbol{p}_D$, the point on the domain closest to the TS,

$$\boldsymbol{p}_D = \boldsymbol{p}_{TS} + \begin{bmatrix} \cos(\alpha) \\ \sin(\alpha) \end{bmatrix} l, \tag{19}$$

and $\boldsymbol{p}_B$, the point on the domain closest to the OS,

$$\boldsymbol{p}_B := \boldsymbol{p}_D + (\boldsymbol{p} - \boldsymbol{p}_D)^\top \boldsymbol{n}_{p_D} \boldsymbol{n}_{p_D}, \tag{20}$$

where

$$\boldsymbol{n}_{p_D} = \begin{bmatrix} \cos(\alpha + \frac{\pi}{2}) \\ \sin(\alpha + \frac{\pi}{2}) \end{bmatrix} \tag{21}$$

is the tangent unit vector to the TS domain. An illustration of the TS domain is given in Figure 7 for two instances of the ownship, denoted OS and OS', one located on each side of the port-starboard split angle α_s.

Figure 8 shows a grid with normal vectors to the TS domain for an OS located at the base of each normal vector. The port-starboard split angle α_s is indicated by an orange line. The effect of the deflection angle α_d is apparent from the vector field close to the orange line, where it will cause the OS to deflect to one or the other side.

The effect of the saturation of α_D is also apparent from the unidirectional vector-field in the top right and top left parts of the overtaking, head-on, and give-way vector fields. The saturation limits on α_D are applied to ensure that the OS maintains a give-way maneuver until it is finally past and clear, in particular to prevent the OS from moving into the path of the TS at close range after an

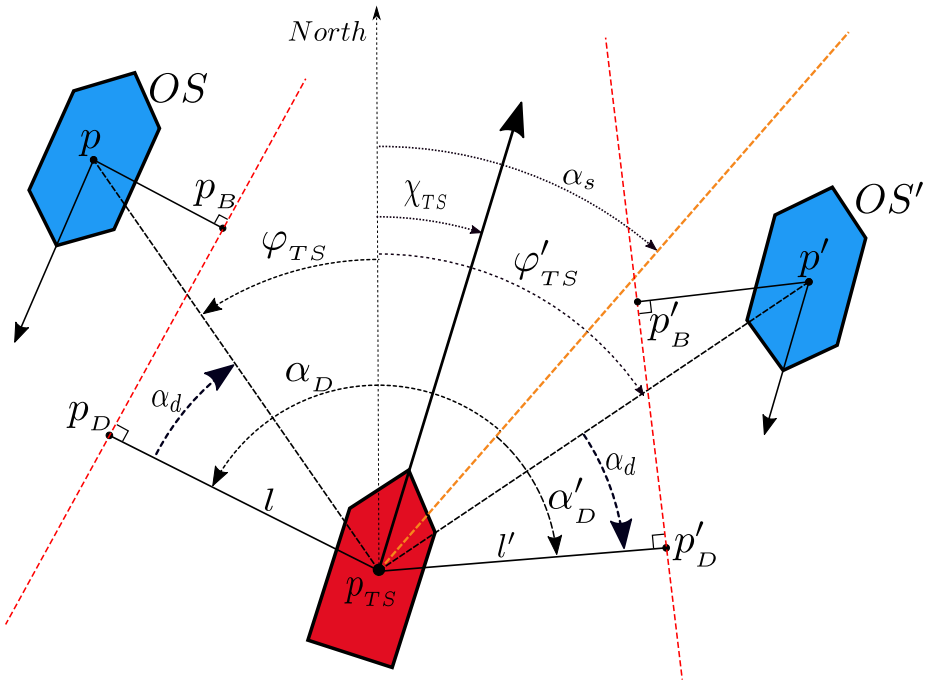

Figure 7. Parameters for the TS domain for a red TS located at $\boldsymbol{p}_{TS}$ with course χ_{TS}, and two instances of the OS, namely OS and OS', located at p and p' at either side of the orange port-starboard split line defined by α_s, with bearing from the TS φ_{TS} and φ'_{TS}, respectively. The TS domain is given by the red dashed line passing through $\boldsymbol{p}_D$ and $\boldsymbol{p}'_D$ at a distance $l > r_{dyn}$ from the center of the TS. The points $\boldsymbol{p}_B$ and $\boldsymbol{p}'_B$ are the closest points on the TS domain to the OS and OS', respectively. All angles are positive in the clockwise direction.

overtaking maneuver. Additionally, with the use of a high deflection angle α_d, in combination with effective saturation limits on α_D, we can achieve an extended effective TS domain in the desired directions. This is apparent from Figure 8, where the TS domain extends aft of the TS in overtaking encounters, in front of the TS in head-on encounters, and to the front and either side of the TS in give-way crossing encounters, without ineffective extensions of the TS domain that only contribute to restricting the maneuverable space. The TS domain that we propose is in line with choosing a TS domain in such a way that when contouring, the OS behaves in accordance with protocol.

The safe set regarding all dynamic obstacles is defined as the complement set of the sum of the unsafe sets. That is,

$$\mathcal{C}_{dyn} = \mathcal{C}^c_{u\_dyn}, \tag{22}$$

with

$$\mathcal{C}_{u\_dyn} := \sum_{i=1}^{N_{TS}} \mathcal{C}_{u\_dyn\_i}, \tag{23}$$

where $\mathcal{C}_{u\_dyn\_i}$ is the domain of TS i. The set $\mathcal{C}_{dyn}$ is convex.

5. Static obstacle domain

Confined waters operations require consideration of the available maneuverable space when moving in proximity to other vessels, in addition to active COLAV regarding static obstacles. Unexpected maneuvers by a TS during a close quarter passing can move the TS domain closer to the OS, and hence push the OS towards static obstacles. Additionally, the position and size of the static obstacles

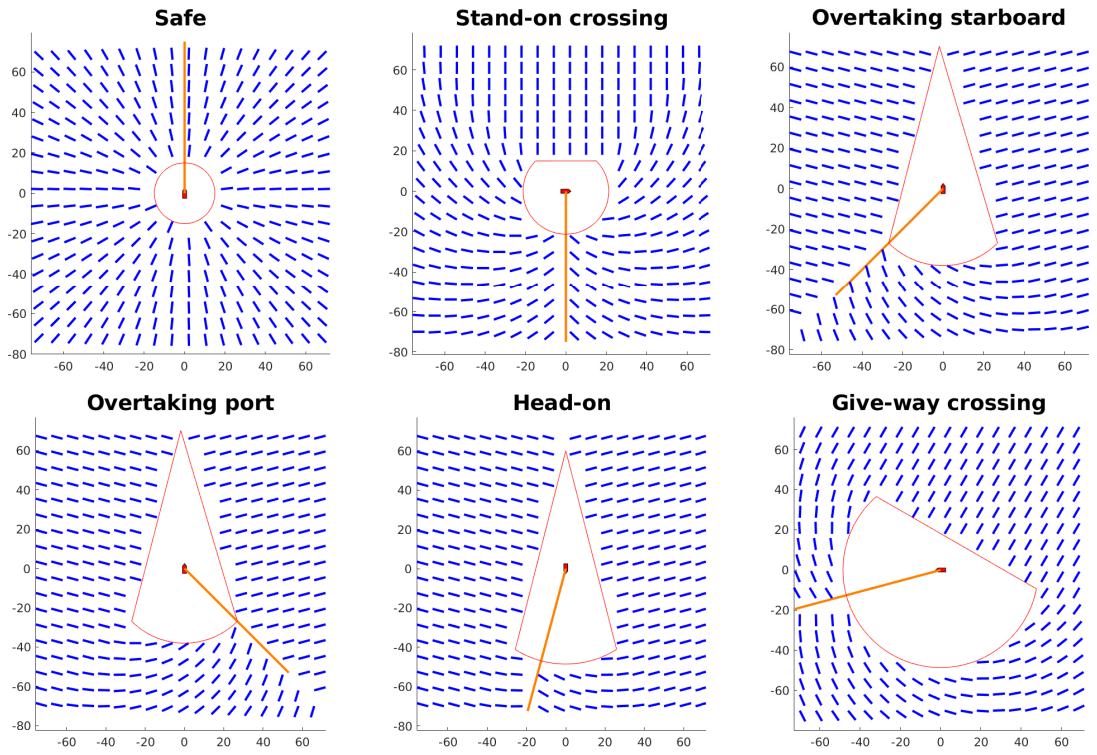

Figure 8. Illustration of the TS domain. In blue, a vector-field of normal vectors to the TS domain for an OS located at the base of each vector. The OS has its heading aligned with its course at $\chi = 0$ and speed of $1\,\mathrm{m/s}$. The orange line indicates the port-starboard split angle α_s and the red contour around the TS indicates the shortest allowable range to the TS at any approach angle.

in the map might differ from the reality due to quasistatic features such as docked or stationary vessels, or floating harbors that change position as a result of periodic water movements or other external forces.

We propose to handle static obstacles in a similar way to dynamic obstacles, where first a set of relevant static obstacles is determined, then a domain is assigned to each of the relevant static obstacles, and lastly we try to avoid entering that domain. To determine the set of relevant static obstacles, we apply a simple approach that is general and applicable for most map data, and most importantly is easily unifiable with real-time lidar data, which we will apply in the experiments to mitigate the effects of unprecise map data as well as estimation errors in the vessel's navigation system.

First, the area around the OS is split into n_{sect} equally sized sectors, with the OS as the center. Subsequently, the closest point on any of the map-entries and the closest point for a lidar measurement within each sector are found. Of these two points, the one that is closest to the OS is considered the relevant static obstacle in that sector. For sector i, this point is denoted $\boldsymbol{p}_{stat\_i} \in \mathbb{R}^2$. The method for finding the closest point in each sector should be chosen to match the specific map data, e.g., for map data consisting of convex polygons it can be computed at a considerably lower cost than for nonconvex polygons (Atallah et al., 1991).

We then define a domain for each point, $\boldsymbol{p}_{stat\_i}$. The domain has the same form as for dynamic obstacles, with a straight line that divides the northeast plane into two halves. When determining the orientation, and hence a normal vector to the domain line, the method presented in (Martinsen et al., 2020) is applied. The method calculates the tangent vector to the domain line for each point $\boldsymbol{p}_{stat\_i}$ so that it is tangent to an ellipse around the OS, where the major axis of the ellipse is

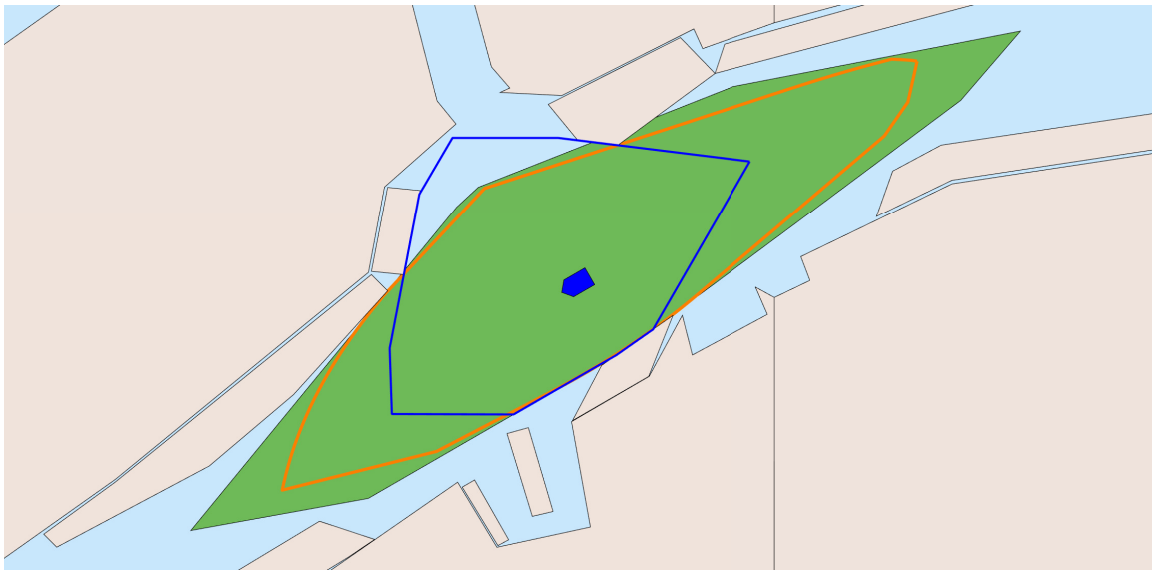

Figure 9. The green polygon gives the set $\mathcal{C}_{stat}$ for $n_{sect} = 12$. The boundary of a more refined set with $n_{sect} = 2000$ is given by the orange graph. The set with $n_{sect} = 12$ gives a sufficiently good $\mathcal{C}_{stat}$, with reduced computational cost compared to a high n_{sect}. The blue graph is the boundary of a set with $n_{sect} = 12$, where the normal vector for domain i is aligned with the vector from the $\boldsymbol{p}_{stat\_i}$ to $\boldsymbol{p}$. The benefit of the method from (Martinsen et al., 2020) is apparent, as it gives a $\mathcal{C}_{stat}$ that is more open in the desired direction of travel.

aligned with the desired OS course from the guidance system. The safe set regarding static obstacles is defined as the complement set of the unsafe set, that is,

$$\mathcal{C}_{stat} = \mathcal{C}_{u\_stat}^{c} \tag{24}$$

with

$$\mathcal{C}_{u\_stat} := \sum_{i=1}^{n_{sect}} \mathcal{C}_{u\_stat\_i}, \tag{25}$$

where $\mathcal{C}_{u\_stat\_i}$ is the unsafe set to the point $\boldsymbol{p}_{stat\_i}$. The set $\mathcal{C}_{stat}$ is by design a convex set in $\mathbb{R}^2$. In Figure 9, $\mathcal{C}_{stat}$ is illustrated for the vessel in blue, with the parameters from Table 2. The green polygon is $\mathcal{C}_{stat}$ for the OS in blue with $n_{sect} = 12$, while the orange line indicates a more refined set, with $n_{sect} = 2000$. The set approximated by $n_{sect} = 12$ gives a sufficiently good approximation, and will greatly reduce the computational cost compared to a higher n_{sect} by reducing both the number of lookups in map data and the number of inequality constraints in the optimization problem that will be defined later. From the figure, the effect of choosing domain tangent angles according to (Martinsen et al., 2020) is also apparent, where the blue graph shows the boundary of a set for $n_{sect} = 12$, but the domain tangent vector instead is made tangent to a circle around the OS. The figure shows that $\mathcal{C}_{stat}$ is stretched out along the canal, which is the desired direction of travel. This reduces the chance of $\mathcal{C}_{stat}$ being restricted so much by obstacles to either side in front of the OS as to totally obstruct further transit along the reference path, which improves the COLAV method's ability to traverse highly confined areas.

6. Safe set and CBF synthesis

The safe operating set of the OS can now be defined as

$$\mathcal{C} := \{\boldsymbol{p} \mid \boldsymbol{p} \in \mathcal{C}_{dyn} \wedge \boldsymbol{p} \in \mathcal{C}_{stat}\}, \tag{26}$$

where we consider the vessel to be safe from collision and maneuvering in compliance with the mentioned COLREGs rules as long as it stays within this set. In this section, we introduce the means of forward invariance of $\mathcal{C}$, namely the CBF. In the following subsections, we will formulate the CBFs for both dynamic and static obstacles, such that the combined set of CBFs will ensure that $\boldsymbol{p}$ stays in $\mathcal{C}$ by restricting the control inputs. In the CBF formulation we apply the 3DOF vessel model from (Fossen, 2011), with

$$\dot{\boldsymbol{p}} = \boldsymbol{R}_\psi \boldsymbol{\nu}, \tag{27}$$

$$\dot{\boldsymbol{\nu}} = \boldsymbol{M}^{-1}\left(\boldsymbol{C}(\boldsymbol{\nu})\boldsymbol{\nu} + \boldsymbol{D}(\boldsymbol{\nu})\boldsymbol{\nu}\right) + \boldsymbol{M}^{-1}\boldsymbol{\tau}, \tag{28}$$

where $\boldsymbol{M}$ is the inertia matrix including hydrodynamic added mass, $\boldsymbol{C}(\boldsymbol{\nu})$ is the Coriolis-centripetal matrix, $\boldsymbol{D}(\boldsymbol{\nu})$ is the damping matrix, $\boldsymbol{\tau} \in \mathbb{R}^3$ are the generalized forces produced by the actuators, and

$$\boldsymbol{R}_\psi = \begin{bmatrix} \cos(\psi) & -\sin(\psi) & 0 \\ \sin(\psi) & \cos(\psi) & 0 \end{bmatrix}. \tag{29}$$

6.1. CBF for dynamic obstacles

The CBFs for dynamic obstacles are formulated with respect to each TS domain at the current time. In the formulation, we do not consider the dynamics of the domain. The domain can therefore be considered as a straight line moving in $\mathbb{R}^2$ with a constant velocity and a constant rate of rotation about the point $\boldsymbol{p}_{TS}$, hence the effects on the domain dynamics from the accelerations of the OS $\ddot{\boldsymbol{p}}$ are omitted. The reasons for this will be discussed shortly.

It is with respect to the point $\boldsymbol{p}_B$ that we define the CBF as

$$h_{dyn}(\boldsymbol{x}) := \boldsymbol{n}_{\tilde{p}}^\mathsf{T}\tilde{\boldsymbol{p}} + c_{dyn}\boldsymbol{n}_{\tilde{p}}^\mathsf{T}\dot{\tilde{\boldsymbol{p}}}, \tag{30}$$

where $\boldsymbol{x} = [\boldsymbol{p}^\mathsf{T}, \dot{\boldsymbol{p}}^\mathsf{T}, \boldsymbol{p}_{TS}^\mathsf{T}, \dot{\boldsymbol{p}}_{TS}^\mathsf{T}, \chi_{TS}]^\mathsf{T} : \mathbb{R}^2 \times \mathbb{R}^2 \times \mathbb{R}^2 \times \mathbb{R}^2 \times \mathbb{S}$,

$$\tilde{\boldsymbol{p}} = \boldsymbol{p} - \boldsymbol{p}_B, \tag{31}$$

and

$$\boldsymbol{n}_{\tilde{p}} = \begin{bmatrix} \cos(\alpha) \\ \sin(\alpha) \end{bmatrix} \tag{32}$$

is the unit vector of $\tilde{\boldsymbol{p}}$. The first and second terms in (30) are the Euclidean distance to and the relative velocity towards the TS domain, respectively, where the parameter $c_{dyn} > 0$ mitigates between the distance to the domain and the velocity at which the OS is allowed to approach the domain. The parameter c_{dyn} serves as a direct method of setting a threshold for how early the OS should start to maneuver in an encounter. This is illustrated by the simulations presented in Figure 10, where the parameter demonstrates its suitability for enforcing the parts of Rule 8 concerning making maneuvers "in ample time." The parameter c_{dyn} should also reflect the physical aspect of the vessel as discussed by the authors in a previous work (Thyri et al., 2020a).

To apply the CBF as an inequality constraint in the quadratic program (QP), we need it on the affine form in (4). Hence, we need the time-derivative of $h_{dyn}(\boldsymbol{x})$,

$$\dot{h}_{dyn}(\boldsymbol{x}) = \dot{\boldsymbol{n}}_{\tilde{p}}^\mathsf{T}\tilde{\boldsymbol{p}} + \boldsymbol{n}_{\tilde{p}}^\mathsf{T}\dot{\tilde{\boldsymbol{p}}} + c_{dyn}(\dot{\boldsymbol{n}}_{\tilde{p}}^\mathsf{T}\dot{\tilde{\boldsymbol{p}}} + \boldsymbol{n}_{\tilde{p}}{}^\mathsf{T}\ddot{\tilde{\boldsymbol{p}}}), \tag{33}$$

with $\dot{\tilde{\boldsymbol{p}}} = \dot{\boldsymbol{p}} - \dot{\boldsymbol{p}}_B$, where $\dot{\boldsymbol{p}} = [\dot{N}, \dot{E}]^\mathsf{T}$ is the northeast velocity of the OS, and

$$\dot{\boldsymbol{n}}_{\tilde{p}} = \frac{\partial \boldsymbol{n}_{\tilde{p}}}{\partial \alpha}\dot{\alpha}. \tag{34}$$

Further,

$$\begin{aligned} \dot{\boldsymbol{p}}_B =& \dot{\boldsymbol{p}}_D + (\dot{\boldsymbol{p}} - \dot{\boldsymbol{p}}_D)^\mathsf{T}\boldsymbol{n}_{p_D}\boldsymbol{n}_{p_D} + (\boldsymbol{p} - \boldsymbol{p}_D)^\mathsf{T}\dot{\boldsymbol{n}}_{p_D}\boldsymbol{n}_{p_D} \\ &+ (\boldsymbol{p} - \boldsymbol{p}_D)^\mathsf{T}\boldsymbol{n}_{p_D}\dot{\boldsymbol{n}}_{p_D}, \end{aligned} \tag{35}$$

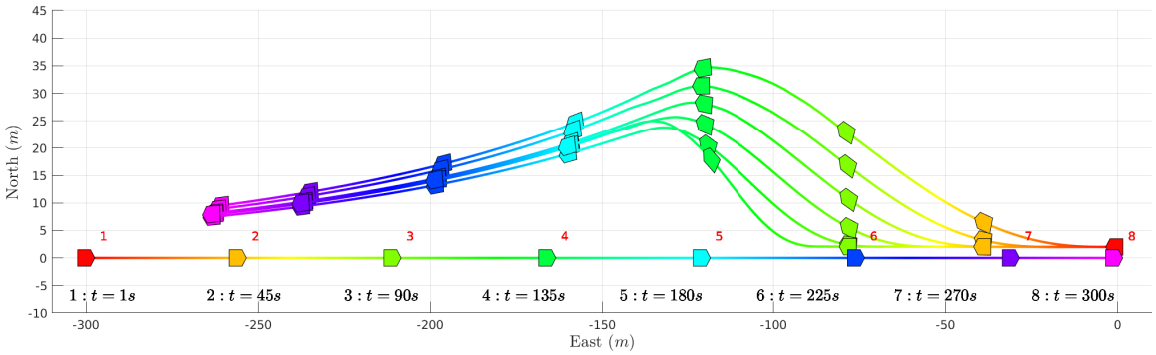

Figure 10. Simulations from a head-on encounter with varying values of c_{dyn}. The TS is traveling east and the OS is traveling west, at parallel paths with a 2 m separation. Both vessels have a speed of 1 m/s. The six OS trajectories are for $c_{dyn} = [10, 30, 50, 70, 90, 110]$, where the southernmost trajectory has $c_{dyn} = 10$, and the northernmost one has $c_{dyn} = 110$.

where

$$\dot{\boldsymbol{n}}_{p_D} = \frac{\partial \boldsymbol{n}_{p_D}}{\partial \alpha}\dot{\alpha}, \tag{36}$$

and

$$\dot{\boldsymbol{p}}_D = \dot{\boldsymbol{p}}_{TS} + \begin{bmatrix} -\sin(\alpha) \\ \cos(\alpha) \end{bmatrix} l\dot{\alpha} \tag{37}$$

is the derivative of (19). In the CBF formulation, we assume that the TS maintains a constant course and speed, and hence

$$\dot{\alpha} = \begin{cases} \dot{\varphi}_{TS} & \text{if } \alpha_D \text{ is not in saturation,} \\ 0 & \text{if } \alpha_D \text{ is in saturation,} \end{cases} \tag{38}$$

with

$$\dot{\varphi}_{TS} = \left(\boldsymbol{R}_2(\tfrac{\pi}{2}) \frac{\bar{\boldsymbol{p}}}{\bar{\boldsymbol{p}}^{\mathsf{T}}\bar{\boldsymbol{p}}} \right)^{\mathsf{T}} \dot{\bar{\boldsymbol{p}}}, \tag{39}$$

where $\dot{\bar{\boldsymbol{p}}} = \dot{\boldsymbol{p}} - \dot{\boldsymbol{p}}_{TS}$ denotes the relative velocity between the two vessels, and

$$\boldsymbol{R}_2(\phi) = \begin{bmatrix} \cos(\phi) & -\sin(\phi) \\ \sin(\phi) & \cos(\phi) \end{bmatrix}. \tag{40}$$

Lastly, from (33), we need the double time derivative of $\tilde{\boldsymbol{p}}$. In the calculations of $\ddot{\bar{\boldsymbol{p}}} = \ddot{\boldsymbol{p}} - \ddot{\boldsymbol{p}}_B$, we set $\ddot{\boldsymbol{p}}_B = \boldsymbol{0}$, since the acceleration of the TS domain is omitted. This is done in order to facilitate a desired behavior when close to the domain. By setting $\ddot{\boldsymbol{p}}_B = \boldsymbol{0}$, the resulting gradient of the CBF is rotated in the direction of the deflection angle, which facilitates the OS to traverse in that direction. This gives $\ddot{\bar{\boldsymbol{p}}} = \ddot{\boldsymbol{p}}$, where

$$\begin{aligned} \ddot{\boldsymbol{p}} &= \frac{\partial \boldsymbol{R}_\psi}{\partial \psi}\dot{\psi}\boldsymbol{\nu} - \boldsymbol{R}_\psi \boldsymbol{M}^{-1}\left(\boldsymbol{C}(\boldsymbol{\nu})\boldsymbol{\nu} + \boldsymbol{D}(\boldsymbol{\nu})\boldsymbol{\nu}\right) + \boldsymbol{R}_\psi \boldsymbol{M}^{-1}\boldsymbol{\tau} \\ &= \boldsymbol{F}_{\ddot{p}} + \boldsymbol{G}_{\ddot{p}}\boldsymbol{\tau}, \end{aligned} \tag{41}$$

with

$$\boldsymbol{F}_{\ddot{p}} = \frac{\partial \boldsymbol{R}_\psi}{\partial \psi}\dot{\psi}\boldsymbol{\nu} - \boldsymbol{R}_\psi \boldsymbol{M}^{-1}\left(\boldsymbol{C}(\boldsymbol{\nu})\boldsymbol{\nu} + \boldsymbol{D}(\boldsymbol{\nu})\boldsymbol{\nu}\right) \tag{42}$$

and

$$\boldsymbol{G}_{\ddot{p}} = \boldsymbol{R}_{\psi}\boldsymbol{M}^{-1}\boldsymbol{\tau}, \tag{43}$$

By inserting for (41) into (33), the CBF derivative takes the form

$$\begin{aligned}\dot{h}(\boldsymbol{x}) &= \dot{\boldsymbol{n}}_{\tilde{p}}^{\mathsf{T}}\tilde{\boldsymbol{p}} + \boldsymbol{n}_{\tilde{p}}^{\mathsf{T}}\dot{\tilde{\boldsymbol{p}}} + c_{dyn}\left(\dot{\boldsymbol{n}}_{\tilde{p}}^{\mathsf{T}}\dot{\tilde{\boldsymbol{p}}} + \boldsymbol{n}_{\tilde{p}}{}^{\mathsf{T}}\boldsymbol{F}_{\ddot{p}}\right) + c_{dyn}\dot{\boldsymbol{n}}_{\tilde{p}}^{\mathsf{T}}\boldsymbol{G}_{\ddot{p}}\boldsymbol{\tau} \\ &= \boldsymbol{F}_{\dot{h}} + \boldsymbol{G}_{\dot{h}}\boldsymbol{\tau},\end{aligned} \tag{44}$$

with

$$\boldsymbol{F}_{\dot{h}} = \dot{\boldsymbol{n}}_{\tilde{p}}^{\mathsf{T}}\tilde{\boldsymbol{p}} + \boldsymbol{n}_{\tilde{p}}^{\mathsf{T}}\dot{\tilde{\boldsymbol{p}}} + c_{dyn}\left(\dot{\boldsymbol{n}}_{\tilde{p}}^{\mathsf{T}}\dot{\tilde{\boldsymbol{p}}} + \boldsymbol{n}_{\tilde{p}}{}^{\mathsf{T}}\boldsymbol{F}_{\ddot{p}}\right) \tag{45}$$

and

$$\boldsymbol{G}_{\dot{h}} = c_{dyn}\dot{\boldsymbol{n}}_{\tilde{p}}^{\mathsf{T}}\boldsymbol{G}_{\ddot{p}}, \tag{46}$$

which is affine in the control input $\boldsymbol{\tau}$. From (44), we can formulate an inequality constraint on the form of (4) as

$$\boldsymbol{F}_{\dot{h}} + \boldsymbol{G}_{\dot{h}}\boldsymbol{\tau} \geq -\gamma(h_{dyn}(\boldsymbol{x})), \tag{47}$$

which can be applied as an inequality constraint in an optimization problem on the form $A\boldsymbol{\tau} \leq b$, with

$$A = -\boldsymbol{G}_{\dot{h}}, \tag{48}$$

$$b = \gamma(h_{dyn}(\boldsymbol{x})) + \boldsymbol{F}_{\dot{h}}. \tag{49}$$

6.2. CBF for static obstacles

For static obstacles, a similar CBF is formulated. The CBF takes the same form as for dynamic obstacles,

$$h_{stat}(x) = \boldsymbol{n}_{stat}^{\mathsf{T}}\tilde{\boldsymbol{p}}_{stat} + c_{stat}\boldsymbol{n}_{stat}^{\mathsf{T}}\dot{\tilde{\boldsymbol{p}}}_{stat}, \tag{50}$$

where $\boldsymbol{n}_{stat}$ is the normal vector to the domain assigned to $\boldsymbol{p}_{stat}$ and $\tilde{\boldsymbol{p}}_{stat} = \boldsymbol{p} - \boldsymbol{p}_{stat}$. Since $\dot{\boldsymbol{n}}_{stat} = 0$ and $\dot{\boldsymbol{p}}_{stat} = 0$, the CBF derivative takes the simple form

$$\dot{h}_{stat}(\boldsymbol{x}) = \boldsymbol{n}_{stat}^{\mathsf{T}}\dot{\boldsymbol{p}} + c_{stat}\boldsymbol{n}_{stat}^{\mathsf{T}}\ddot{\boldsymbol{p}}. \tag{51}$$

By inserting (41) into (51), we get

$$\dot{h}_{stat}(\boldsymbol{x}) = \boldsymbol{n}_{stat}^{\mathsf{T}}\dot{\boldsymbol{p}} + c_{stat}\boldsymbol{n}_{stat}^{\mathsf{T}}\left(\boldsymbol{F}_{\ddot{p}} + \boldsymbol{G}_{\ddot{p}}\boldsymbol{\tau}\right), \tag{52}$$

which again can be put in the form of (4) as

$$\boldsymbol{F}_{\dot{h}_{stat}} + \boldsymbol{G}_{\dot{h}_{stat}}\boldsymbol{\tau} \geq -\gamma(h(\boldsymbol{x})_{stat}) \tag{53}$$

with

$$\boldsymbol{F}_{\dot{h}_{stat}} = \dot{\boldsymbol{p}}^{\mathsf{T}}\boldsymbol{n}_{stat} + c_{stat}\boldsymbol{n}_{stat}^{\mathsf{T}}\boldsymbol{F}_{\ddot{p}} \tag{54}$$

and

$$\boldsymbol{G}_{\dot{h}_{stat}} = c_{stat}\boldsymbol{n}_{stat}^{\mathsf{T}}\boldsymbol{G}_{\ddot{p}}. \tag{55}$$

The inequality of (53) can be applied as a constraint in an optimization problem in the same form as (47).

Table 1. Rule-based parameters for the TS domain.

Parameter	*SF*	*SO*	OT_p	*OTs*	*HO*	*GW*	Unit
α_d	0	$\pi/4$	$\pi/3$	$\pi/3$	$2\pi/5$	$2\pi/5$	rad
α_s	0	$\pi/2$	$-3\pi/4$	$3\pi/4$	$\pi/12$	$-\pi/8$	rad
α_{D_max}	π	π	$\pi/3$	$5\pi/6$	$\pi/2$	$2\pi/5$	rad
α_{D_min}	$-\pi$	$-\pi$	$-5\pi/6$	$-\pi/3$	$-2\pi/3$	$-6\pi/5$	rad
c_{dyn}	10	10	40	40	60	60	s
δ_{dyn}	1	1	4	4	1	1	m

6.3. Application to the GNC pipeline

To apply the constraints from the CBFs, a quadratic problem is formulated as

$$\begin{aligned} \min_{\boldsymbol{\tau}} \quad & \frac{1}{2}(\boldsymbol{\tau}-\boldsymbol{\tau}_d)^\top \boldsymbol{K}_\tau(\boldsymbol{\tau}-\boldsymbol{\tau}_d), \\ \text{s.t.} \quad & \dot{\mathcal{H}}_{dyn} \text{ and} \\ & \dot{\mathcal{H}}_{stat}, \end{aligned} \tag{56}$$

where $\boldsymbol{K}_\tau > 0$ is a 3 by 3 weighting matrix, $\dot{\mathcal{H}}_{dyn}$ and $\dot{\mathcal{H}}_{stat}$ are the set of inequalities from (47) and (53) for all dynamic and static obstacles, respectively, and $\boldsymbol{\tau}_d \in \mathbb{R}^3$ is a desired virtual force that can be provided by an arbitrary controller that is suitable for the control objective. Additional constraints are applied to ensure that the actuator magnitude constraints are overheld. The resulting $\boldsymbol{\tau}$ should be realized without further steps in the GNC pipeline to ensure the integrity of the proposed method. If the system is prone to allocation errors from, e.g., thruster dynamics such as rate-constraints or thruster deadband, the thruster dynamics should be included in the vessel model, as proposed in (Basso et al., 2020), where the QP solves the trajectory tracking, COLAV, and thrust allocation.

7. Simulations

In this section, the simulation results are presented. First, an extensive set of simple V2V encounters in open waters is presented and discussed. The motivation for this is to demonstrate the effectiveness and completeness of the proposed TS domain. Thereafter, we include a set of three simulations in complex environments with up to three maneuvering vessels. In these simulations, two or more of the vessels are running the proposed COLAV method. The intent of these simulations is to demonstrate the method as a whole, and show that it is suitable for multiagent operation. Lastly, we demonstrate the capacity of the method, and we provide some remarks on runtime through a simulation with 12 vessels running the proposed COLAV method. The simulations are run in a simulator implemented in Matlab with a 3DOF vessel model of the milliAmpere experimental platform depicted in Figures 1 and 19a. The model parameters used in the simulations are estimated based on a data-driven approach through the work presented in (Pedersen, 2019). In the simulator, the Matlab ODE45 solver is applied for state integration.

A model of the GNC pipeline with auxiliary systems is visualized in Figure 11. The simulator setup consists of the following modules:

- The **Path Waypoints** module is the input to the system, which is a set of waypoints with corresponding velocities.
- A **LOS Guidance** method with saturated yaw-rate dynamics is applied to calculate the desired course reference

$$\chi_d = \chi + \Delta_t r_d, \tag{57}$$

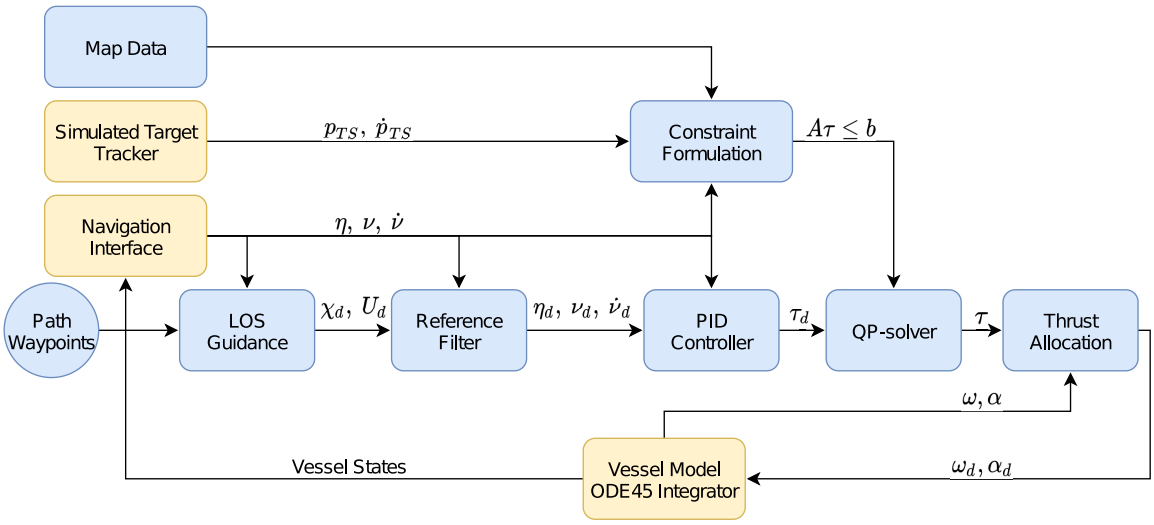

Figure 11. GNC pipeline for simulations. Blue modules are the same in simulations and experiments. Yellow boxes are simulator-specific.

where Δ_t is the run period of the guidance module, and

$$r_d = saturate(\frac{1}{\tau_\chi}(\chi_r - \chi), min_{r_d}, max_{r_d}) \tag{58}$$

is a saturated reference yaw rate, where

$$\chi_r = \theta - \text{atan}(\frac{e}{\Delta}) \tag{59}$$

is a course reference calculated from a constant lookahead distance $\Delta_{lookahead}$, where θ is the course from the previous waypoints to the current waypoint, and e is the cross-track error. This guidance scheme reduces the effect of conflicting objectives between the guidance and the COLAV, compared to simply applying χ_r as a course reference, which is a common approach. This would result in an increasing course error as the OS is maneuvering away from the path in an avoidance maneuver, where the χ_r in the worst case can be perpendicular to a TS domain, resulting in stagnation or a deadlock. The saturated yaw rate reference, and using χ in (57), limits the course error and hence allows the OS to continue an avoidance maneuver until the safe set enables the OS to move back towards the reference path. The rationale behind this is that the COLAV objective has higher priority than the path-following objective.

- A third-order **Reference Filter** is applied to calculate smooth position, velocity, and acceleration references.
- A **PID Controller** with velocity feed-forward performs path following.
- The **Simulated Target Tracker** provides position and velocity states from the other vessels in the simulation.
- The **Navigation Interface** outputs the OS position, velocity, and acceleration.
- The **Map Data** contain all static obstacles in the form of convex polygons.
- The **Constraint Formulation** formulates constraints for all relevant static and dynamic obstacles in accordance with the method presented in Sections 4–6.
- The **QP solver** applies the Matlab solver *mpcqpsolver* to (56).
- The **Thrust Allocation** realizes the virtual force $\boldsymbol{\tau}$ by calculating appropriate setpoints for the two azimuth thrusters according to the method developed by (Torben et al., 2019).

Table 2. Non-rule-based parameters.

Parameter	Value	Parameter	Value
γ_{dyn}	$0.100\,\mathrm{s}^{-1}$	r_{free_max}	40 m
γ_{stat}	$1.00\,\mathrm{s}^{-1}$	k_l	0.50
c_{stat}	5 s	n_{sect}	12
δ_{stat}	6 m	Δ_t	0.05 s
$\Delta_{lookahead}$	100 m	τ_χ	0.2 s
min_{r_d}	-0.5 rad/s	max_{r_d}	0.5 rad/s
$\boldsymbol{K}_\tau$	$diag(1, 1, 1)$	U_{lim}	0.2 m/s

7.1. TS domain validation

We now present results for evaluating the effectiveness of the TS domain. The results are produced through an extensive simulation study, with the OS and TS on straight line paths, where the TS does not maneuver but maintains a constant speed and course. Two parameters have been applied to construct the set of simulations: the relative course χ_{rel} between the vessels, and the lateral offset δ_{lat} of the OS reference path from a point-of-collision at the origin of the local NED frame. The OS and TS waypoints are calculated so that both vessels will be at the origin after 200 s if $\delta_{lat} = 0$. The parameter χ_{rel} is iterated from 0 to 2π at steps of $\pi/16$, while the δ_{lat} is iterated from -300 m to 400 m at 10 m steps, resulting in a total of 2272 simulations. The OS and TS have a reference speed of 1.5 m/s and 1 m/s, respectively. The OS path goes from west to east with a course of $\pi/2$ while the TS path is adjusted for each χ_{rel} so that it passes through the origin. A subset of the simulations is presented in Figure 12, where all OS trajectories for a given TS course are combined in one plot. The full set of figures can be viewed at this OneDrive **repository**.[4]

Figures 12a and 12b show results from encounters where the OS have give-way obligations. From the trajectories, one can see that for most encounters where the OS maneuvers from its nominal path, it adjusts course to starboard to pass behind the TS, in accordance with the protocol. In Figure 12b, the OS starts a small port maneuver along some trajectories before performing a starboard maneuver and passing behind the TS. This is a result of the OS initially being on the positive side of α_s, but it ends up on the negative side as the encounter evolves.

Figures 12c and 12d show results from stand-on encounters. According to protocol, it is the TS that is obliged to give way, where the OS shall keep its course and speed, and only maneuver when it is apparent that the TS is not abiding its duty, and the situation cannot be resolved by maneuvers from the TS alone. This is a difficult evaluation to make, as it requires an understanding of the maneuvering capacity of the TS. Our approach to this is to apply a small c_{dyn} to allow the OS to hold its velocity for longer as the range to the TS domain is reduced. If an understanding of each unique TS was available, this could be used to determine a suitable value for c_{dyn} for each encounter. In the presented simulations, a comparable portion of the simulations maneuvers to pass in front and aft of the TS, due to the choice α_{δ_s}. A preference of passing in front or aft of the TS can be achieved by increasing or decreasing α_{δ_s}, respectively.

Figure 12e shows results from overtaking encounters. The course of the TS relative to the OS favors overtaking with the TS on the port side. At the trajectories for the simulations where the OS starts in the area behind the TS, the OS is able to perform a starboard maneuver to pass behind the TS in the overtaking. At the trajectories where the OS starts further north, it starts on the positive side of the port-starboard split angle and hence adjusts course to port to travel alongside the TS until it can pass clear in front of it. The OS behavior is compliant with Rule 13.

Figures 12f–12h show results from head-on encounters. In most cases where the OS takes action to stay in the safe set, it adjusts course to starboard to pass the TS port to port in compliance with Rule 14. In the head-on simulations where the OS maneuvers and still passes the TS starboard

[4] Full url: https://studntnu-my.sharepoint.com/:f:/r/personal/emilht_ntnu_no/Documents/shared%20data%20publications/cbf_based_colav_journal_paper/batch_simulations?csf=1&web=1&e=Tow8cg

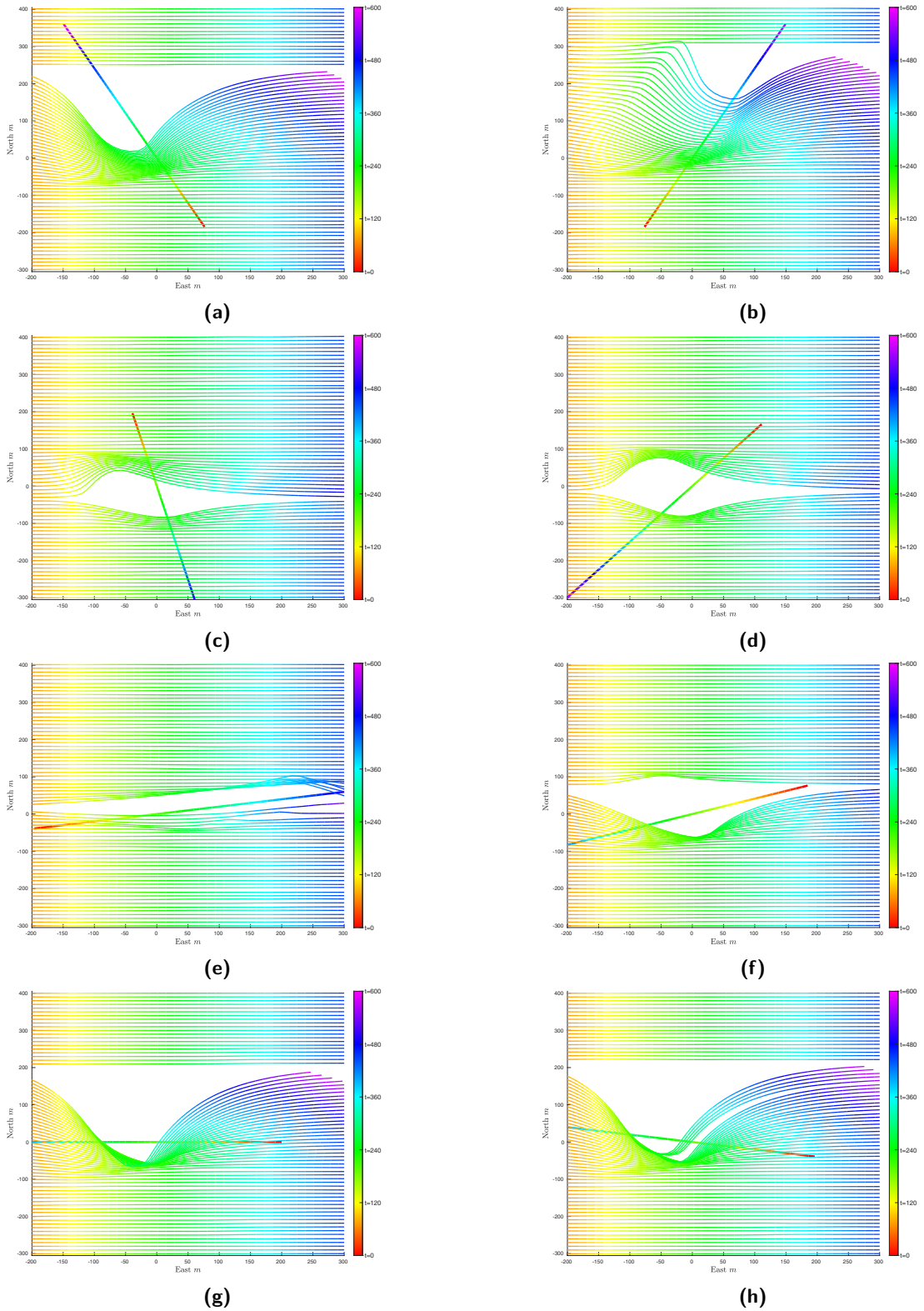

Figure 12. Batches of V2V encounter simulations. In each subfigure, the TS travels along the same trajectory, while the OS trajectory has a varying offset.

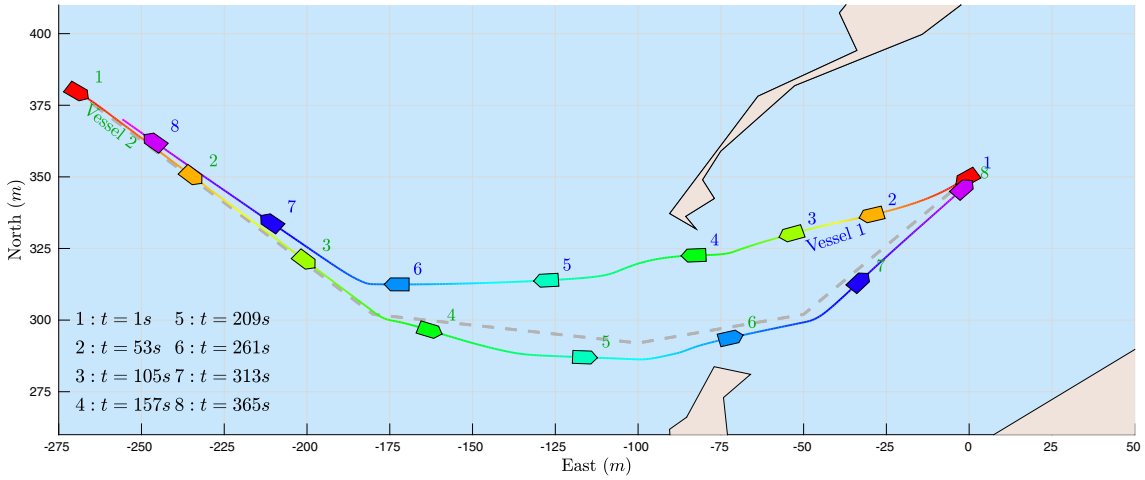

Figure 13. Simulation 1: Harbor area entry: Encounter in entrance to harbor area. Both vessels are autonomous agents, and travel along the same path in opposing directions. Vessels are scaled for visualization.

to starboard, due to the OS initially or by the TS velocity, it appears on the positive side of the port-starboard split angle. In these situations, the OS is in such a position that it will require excessive maneuvering to pass port to port. This is apparent from Figures 12g–12h, where the OS, along some trajectories, maneuvers a long way to starboard in order to pass port to port in cases where keeping a constant course or performing a small port maneuver seems sufficient. Nevertheless, a starboard maneuver is the protocol-compliant maneuver in head-on encounters, where Rule 14 dictates that the two vessels shall pass port to port. The port maneuver from the OS is also excessive due to a lack of maneuvering from the TS, which is also obliged to maneuver and should hence split the maneuvering effort.

7.2. Complex scenarios

We now present results from simulations in complex scenarios with several maneuvering vessels in confined waters with restricted maneuverability.

7.2.1. Head-on: Simulation 1

In Simulation 1, two vessels are meeting in a head-on encounter between two breakwaters in a narrow entry to a harbor area. Both vessels are autonomous agents, and they track the same set of waypoints in the opposite order. The trajectories of the two vessels, as well as the path between the waypoints, are shown in Figure 13. Due to the geometry between the two vessels at the range of static classification, Vessel 1 classifies the encounter as give-way, while Vessel 2 classifies it as a stand-on encounter, despite the vessels in reality being in a head-on encounter. The wrongful classification is held in place by the classification state-machine holding the classification until it is reclassified as safe. Despite the faulty classification, both agents resolve the situation without risk of collision and in accordance with Rule 14 by passing port to port.

The erroneous classification results from the primitive prediction of the TS intention. In the presented work, it is assumed that the TS will maintain a constant course and speed, which is a poor assumption in such confined-water scenarios, where the trajectories of the target ships are very much affected by the presence of static obstacles. By applying knowledge about the operational environment such as typical arrival and departure points and traffic patterns from historical data, a more qualified prediction of the TS trajectory can be made. However, this is outside the scope of this paper, and is left for future work.

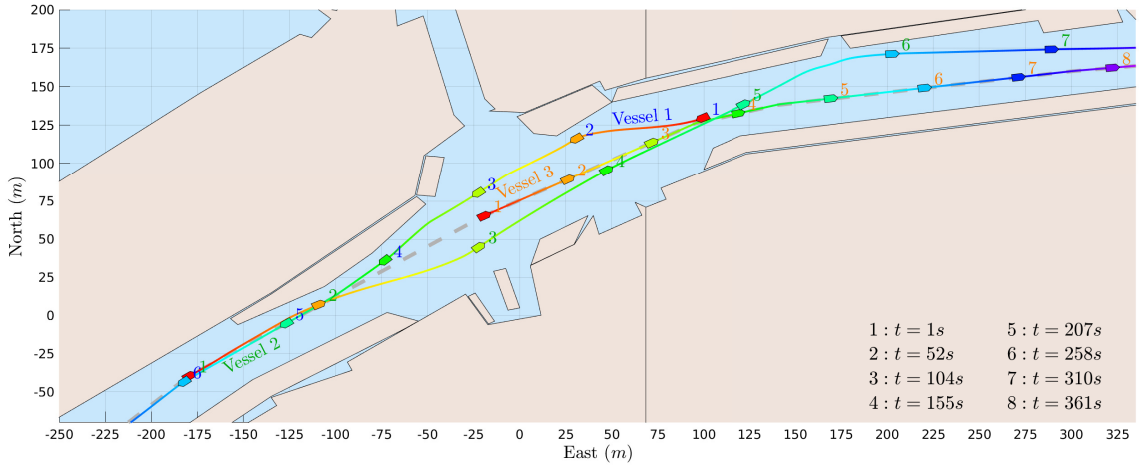

Figure 14. Simulation 2: Multiple encounters in a canal with two autonomous agent vessels and one nonautonomous vessel. All vessels track the same path, indicated by the grey dashed line. Vessels are scaled for visualization.

From the vessel trajectories, one can see that the vessel traveling west initially starts a starboard maneuver to satisfy its give-way duties. The maneuver seems premature from the context, and it is a result of the large TS domain of the east-bound vessel, which initially receives the maximum addition, r_{free_max}, for maneuverable space as it approaches from open waters. The premature starboard maneuver of the west-bound vessel is reduced by CBFs of the static obstacle on its starboard side, as is apparent from the small course adjustments to port between time steps 2 and 3, and the subsequent starboard maneuver as the safe-set opens up just before time step 4. In the same way, the small starboard maneuver of the east-bound vessel puts it at collision risk with the south breakwater, where it performs a small port maneuver between time stamps 5 and 6 to stays in the safe set.

7.2.2. Head-on and overtaking: Simulation 2

In Simulation 2, three vessels are traveling along a canal-area. Vessel 1 and Vessel 2 are autonomous agents, while Vessel 3 is performing simple path following. All vessels track the same set of waypoints, the vessels traveling west in reverse order from the vessels traveling east. The trajectories of the vessels are shown in Figure 14. Vessel 1 is in a head-on encounter with both vessels traveling east. It performs a starboard maneuver and holds its starboard side of the canal to pass both east-bound vessels port to port. Vessel 2 is initially in a head-on encounter with Vessel 1, and subsequently in an overtaking encounter with Vessel 2. It first moves to starboard to pass port to port in the head-on encounter in accordance with Rule 14, and subsequently maneuvers to its port side of the canal to overtake Vessel 3 on its port side due to the relative course of the two vessels, and hence avoid crossing in front of it, in accordance with Rule 13.

Note how Vessel 1 and Vessel 2 split the available space in the overtaking maneuver at time stamp 3, since they both have about the same amount of maneuverable space in their pass-sector. Also note how Vessel 2 keeps well clear during the overtaking maneuver, due to the saturation limits on α_D, visualized by the unidirectional parts of the vector field in Figure 9.

7.2.3. Head-on, overtaking, and crossing: Simulation 3

In Simulation 3, three vessels are traversing a canal system. Vessel 1 and Vessel 2 are traveling west. Vessel 3 enters the canal from the north before traveling east. All vessels are autonomous agents, and they track the same path at the centerline of the canal, where Vessel 3 first tracks a path that merges into the centerline path. The trajectories of the vessels are shown in Figure 15.

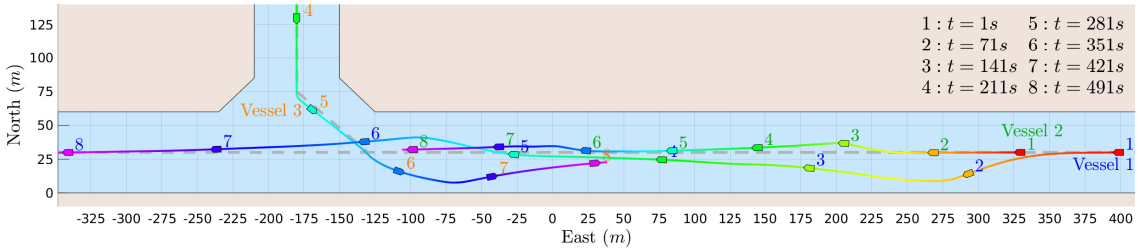

Figure 15. Simulation 3: Multiple encounters where all three vessels are autonomous agents.

Initially, Vessel 1 is in an overtaking encounter and performs an overtaking maneuver on the port side of Vessel 2. As the overtaking comes to an end, Vessel 1 is in a give-way crossing encounter with Vessel 3, and it moves to starboard to pass behind the vessel in accordance with Rule 15. Vessel 2 is initially in a give-way encounter with Vessel 3, but the encounter is reclassified as head-on before the range of static classification is reached, due to the course changes of Vessel 3.

The starboard maneuver of Vessel 2 in the head-on encounter is small due to the speed and heading of Vessel 3 at the time, which in turn restricts the port course-change maneuver of Vessel 3, causing its trajectory to pass close to the south canal bank. The purely reactive features of this method do not provide Vessel 2 with any comprehension of intention of Vessel 3, and hence it does not make a greater maneuvering effort to leave more room.

Note that in all three complex simulations, all the participating vessels track the same nominal path close to the centerline of the waterway, and are hence on a direct collision course with each other at some point along the path. Yet, all encounters are resolved in accordance with protocol. This suggests that the proposer reactive COLAV method, which is intended as a bottom layer method in a hybrid structure, is robust to unfeasible or delayed trajectories from the mid- and top-layer planners, which is of paramount importance for such a system. And, as running the proposed method results in trajectories that are in line with the COLREGs, it will merge well with higher level planners that output trajectories that are in compliance with, or at least do not contradict, the COLREGs.

7.2.4. Traffic capacity and runtime: Simulation 4

The simulations presented up to this point have demonstrated a set of simple yet realistic scenarios for ASV operation in confined waters. The small set of involved vessels allows us to demonstrate a subset of the qualities of the proposed COLAV method in each simulation. However, there are no aspects of the method that make it unsuitable for handling encounters where a higher number of vessels are involved. This is demonstrated through Simulation 4, which involves 12 vessels, where all vessels run the proposed COLAV method. An overview of the simulation is displayed in Figure 16. The high traffic density makes it challenging to comment on the behavior of specific vessels, however all vessels resolve the scenario without collision and in compliance with the COLREGs. The minimum DCPA in the simulation is 25.74 m. From the scenario overview, it is apparent that several of the vessels would benefit from running a hybrid COLAV structure with a more long-term and deliberate planner, as they initiate maneuvers that at a later stage result in situations requiring additional, and sometimes more substantial, maneuvers. In these situations, a more refined initial maneuver might have resolved the scenario without further avoidance maneuvers. However, the scope of this paper concerns a reactive COLAV method, and this simulation demonstrates that the proposed COLAV method can handle high-traffic situations in a safe and COLREGs-compliant manner, and hence ensure the baseline safety of a hybrid COLAV structure.

Since the proposed COLAV method is of a reactive nature, it is important that it has a runtime that allows for real-time operation. In Figure 17, the runtime of the method is displayed for three simulated scenarios, with 3, 8, and 12 vessels, where all vessels run the proposed method. The runtimes are visualized in a normalized histogram. The simulations are run on a single core on a Dell Precision 5540 with a 32 GB memory and an Intel® Core™ i9-9880H processor running at

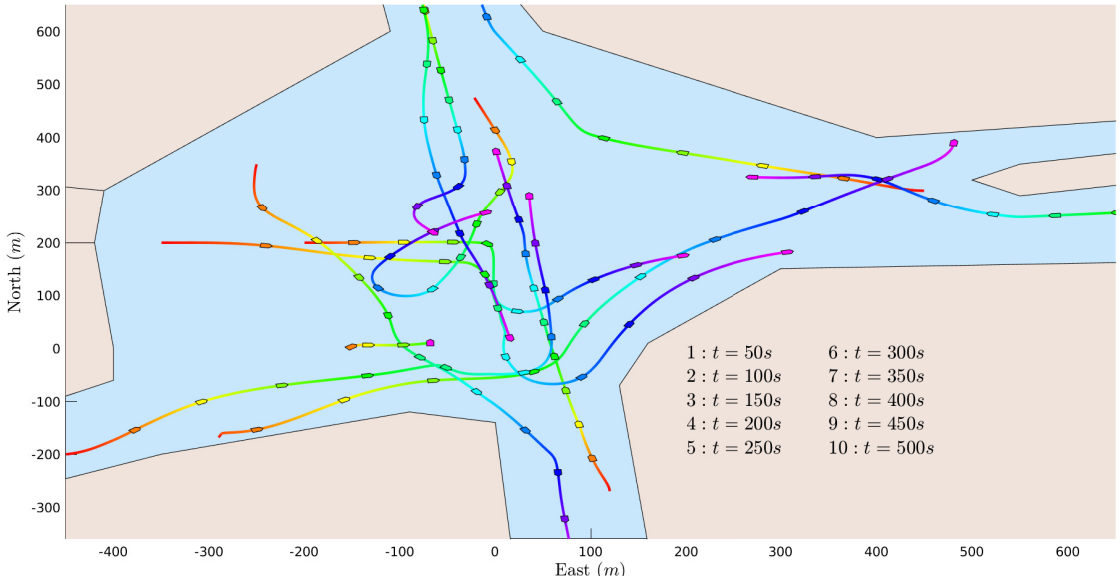

Figure 16. Simulation 4: Crowded waters where all vessels are running the proposed COLAV method. The minimum DCPA for the simulation is 25.74 m.

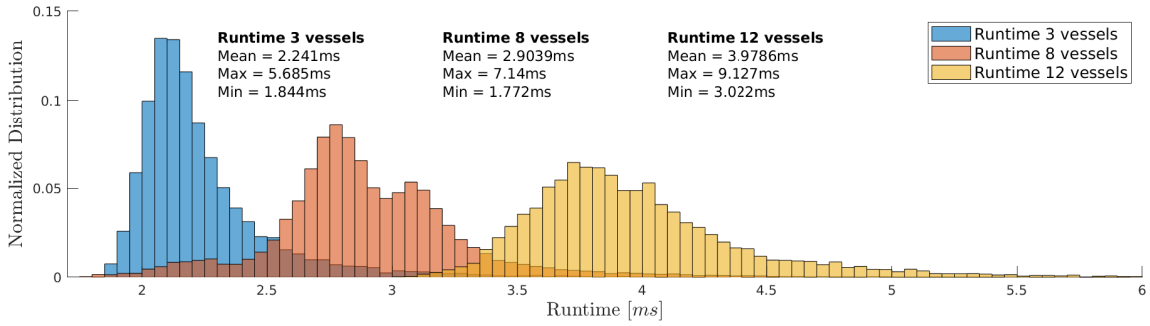

Figure 17. Normalized distribution of runtime for the proposed COLAV algorithm. Results from three simulations with 3, 8, and 12 vessels. The latter is Simulation 4.

2.30 GHz. The code is written in Matlab with no particular regard to runtime optimization, and it runs as a Matlab script. From the figure, one can see that the method has an average runtime between 2 ms and 4 ms, with a worst-case runtime of 9.127 ms. This is more than sufficient for ASV operations, where a suitable run period for a reactive COLAV system would be in the range between 0.1 s and 10 s, depending on the ASV dynamics and the operational environment. For the simulations and experiments in this paper, a run period of 0.1 s was applied.

8. Experiments

The experiments are conducted with the milliAmpere vessel depicted in Figures 1 and 19a. The vessel is a 5 m by 2.8 m prototyping platform hosted by NTNU for developing and testing enabling technology for fully autonomous maritime operations in urban areas. The vessel is fully electric and equipped with two 2KW azimuth thrusters for propulsion. The vessel is also equipped with several sensors for navigation and situational awareness. Relevant hardware is listed in Table 3. The GNC pipeline used in the experiments is visualized in Figure 18, where the green modules are

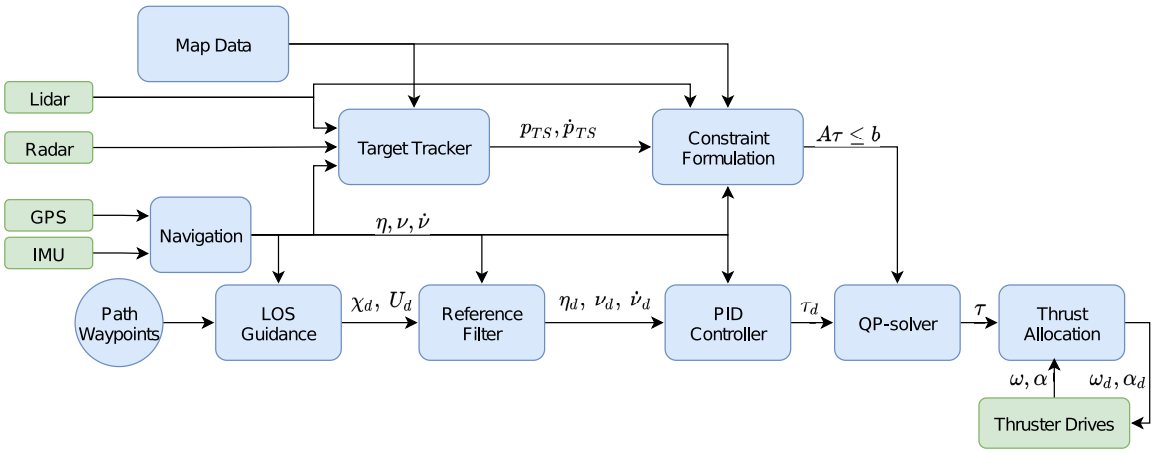

Figure 18. Guidance, navigation, and control pipeline for the experiments. Modules in blue boxes run on the onboard computers. Green boxes are the vessel-mounted equipment.

Table 3. MilliAmpere hardware.

Equipment	Make	Type	Info
Thruster	Torqeedo	Pod Cruise 2.0FP	500 N reversible thrust
Azimuth Servo	Intecno	BLDC	32 deg/sec rotation speed
Onboard computer	Axiomtek	eBOX670-883-FL	I7 processor. Ubuntu with ROS.
GPS system	Vector	VS330	RTK capacity. 10 mm position accuracy
IMU	Xsens	MTi20	Linear acceleration and rate of turn.
Radar	Simrad	Broadband 4G^{TM}	36 RPM
Lidar	Velodyne	Puck / VLP16	100 m range

vessel-mounted hardware, and the blue modules run on one of the onboard computers. The code for the map data, LOS guidance, reference filter, controller, thrust allocation, and QP solver is generated from Simulink to run in ROS.[5]

We apply a lidar- and radar-based target tracker, where an integrated probabilistic data association (IPDA) is used for track initiation and maintenance (Wilthil et al., 2018). The tracker is described in detail in (Wilthil et al., 2017). In (Kufoalor et al., 2019), a further discussion on the tracker and its application to decision support for COLAV is presented, where it is also demonstrated through full-scale experiments in open waters. The output of the target tracker is a list of confirmed tracks, each with a unique ID and an estimate on the target's position and velocity vector.

In initial experiments in the canal, we experienced issues where the tracker confirmed tracks on several of the docked vessels, where clustering and declustering of two or more vessels docked side-by-side resulted in high velocity estimates due to the resultant change in the track's center of mass. We therefore apply a mask to filter out tracks on docked vessels before passing the list of confirmed tracks on to the COLAV system, where tracks under the mask are omitted from the list. The mask was drawn up manually, based on lidar data, and it can be seen in Figures 21–29 as the green field on either side of the canal.

In the experiments, lidar data are used in combination with the map data for COLAV w.r.t. static obstacles. Two stages of filtering are applied to the lidar data. Detections on confirmed tracks are omitted by removing detections within a range of 4 m of the estimated position of the track. Additionally, filtering of single and double detections that are not in proximity to other detections

[5] Robot operating system, https://www.ros.org/about-ros/

(a) milliAmpere **(b)** Havfruen

Figure 19. Vessels used in the experiments.

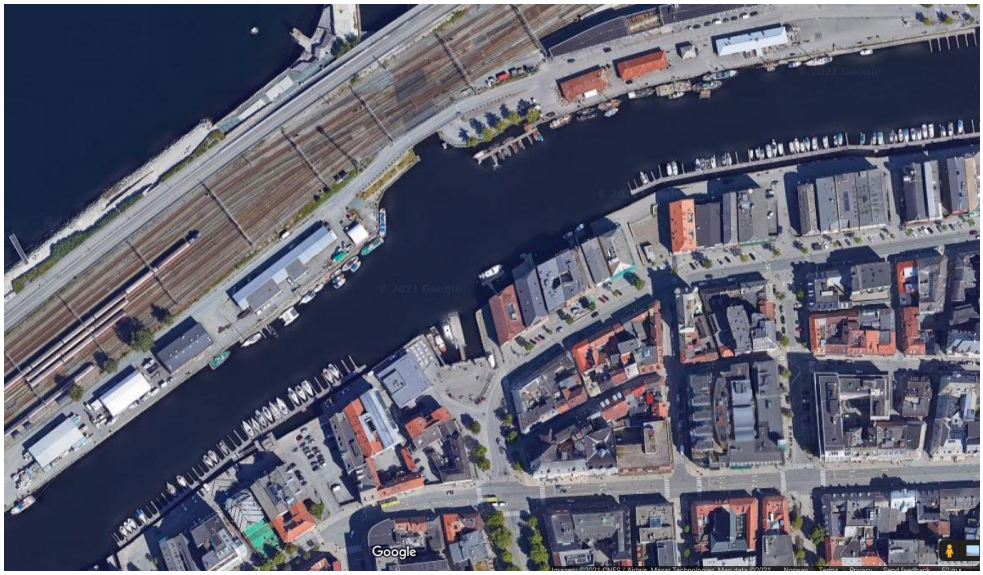

Figure 20. Testing location. Canal area in the northern part of Trondheim.

is omitted. This is done to reduce the risk of noise on the surface of the water, which has been experienced when there is rain, and when the wind causes a certain type of small waves.

The TS used in the experiments is called Havfruen, and it is depicted in Figure 19b. The vessel is a Jeanneau Marlin 695 with a Yamaha 150hp outboard engine. The vessel is equipped with a Garmin eTrex 10 GPS for logging the TS position. There was no information-sharing between the OS and the TS during the experiments.

The experiments were conducted in a canal in the northern part of Trondheim, depicted in Figure 20. The canal is between 60 m and 80 m wide with floating docks on both sides, reducing the free width to 30 m in some places. The location provides a realistic and relevant testing ground for urban ASVs, and it is also the transit location for an urban autonomous passenger ferry pilot project hosted by among others NTNU, Trondheim municipality, and Zeabuz (Stensvold, 2020), where an autonomous ferry will transport pedestrians across the canal.

8.1. Experimental results

Experimental results from nine experiments are presented. Experiments 1.1–1.3 are head-on encounters, experiments 2.1–2.2 are overtaking encounters, and experiments 3.1–3.4 are crossing encounters, where three are give-way crossings and one is a stand-on crossing. All experiments are run in the same area, either along or across the canal. Only one TS, the Havfruen TS (HTS), was used in the experiments, yet the canal is a populated harbor area, and several other docked vessels, as well as false tracks, were detected by the tracker, which in some experiments affected the trajectory of the OS. The data from each experiment are presented through a single figure containing the following information:

- The trajectory of the OS from GPS data, and the estimated trajectory of the controlled HTS, Havfruen, are visualized as thick, colored lines, where the color changes from red, through yellow, green, and blue, to purple as time evolves.
- Vessel representations of the OS and TS tracks at matching 10 s intervals, where the OS representation is a fore-aft symmetric polygon, and the TS representations are flat at the aft. Since the tracker does not provide any size estimates of the tracks, a constant size of 5 m by 3 m is used for all tracks, which is the approximate size of the HTS.
- A scaled-down vessel representation on the recorded GPS position of the HTS, at matching time intervals.
- The trajectories of tracks belonging to docked vessels in the canal that are not filtered by the mask, or false tracks, are plotted as thin colored lines, with vessel representations at matching time steps to the OS and the HTS. However, most tracks belonging to stationary vessels have velocity estimates close to zero, and most false tracks have a very short duration.
- The closest points in each static obstacle sector from the lidar data are visualized as dark red crosses.

Videos showing the time evolvement of the experiment overviews are available at this OneDrive **link**,[6] where additional features such as lidar raw-data, the convex set $\mathcal{C}_{stat}$, and lines indicating the domains of the tracks are visualized.

8.1.1. Head-on: Experiment 1.1

An overview of the experiment is shown in Figure 21, where the OS is traveling east to west, and the HTS is traveling in the opposite direction. The tracker detects a false track for a short period of time close to the point $[N, E] = [-460, -270]$, which causes the OS to start a starboard maneuver to pass in front of the false track. As the false track disappears, the OS continues the starboard maneuver to pass port to port in the head-on encounter with the HTS. As the track on the HTS disappears for approximately 5 s, and then reappears with an initial course pointing more towards the OS, a further increased starboard maneuver is performed by the OS to stay clear of the TS domain of the HTS, before a port maneuver is performed in order to get back on the nominal path and ensure a safe margin to the static obstacles in front of the OS.

The lidar points along the trajectory of the HTS originate from detection on the HTS vessel. These detections should be filtered out from the raw lidar data, as the detections are within the given range of the HTS track position (this is apparent from the video). We believe this fails to happen due to the asynchronous messages in ROS, where sufficient care is not taken to ensure that all tracks are included in the filtering of lidar data. However, this does not affect the performance of the COLAV method, since the restrictions from dynamic obstacles are stricter than for static obstacles. The raw lidar data will therefore only ensure that collision is avoided if the target tracker fails to initiate a track on a vessel, and hence provide redundancy for the target tracker.

[6] Full url: https://studntnu-my.sharepoint.com/:f:/g/personal/emilht_ntnu_no/EnEoh28gB25IjzA8LnxuTWMBPmxI7TFZ-vLYSIzFR1P7dA?e=sHrwWJ

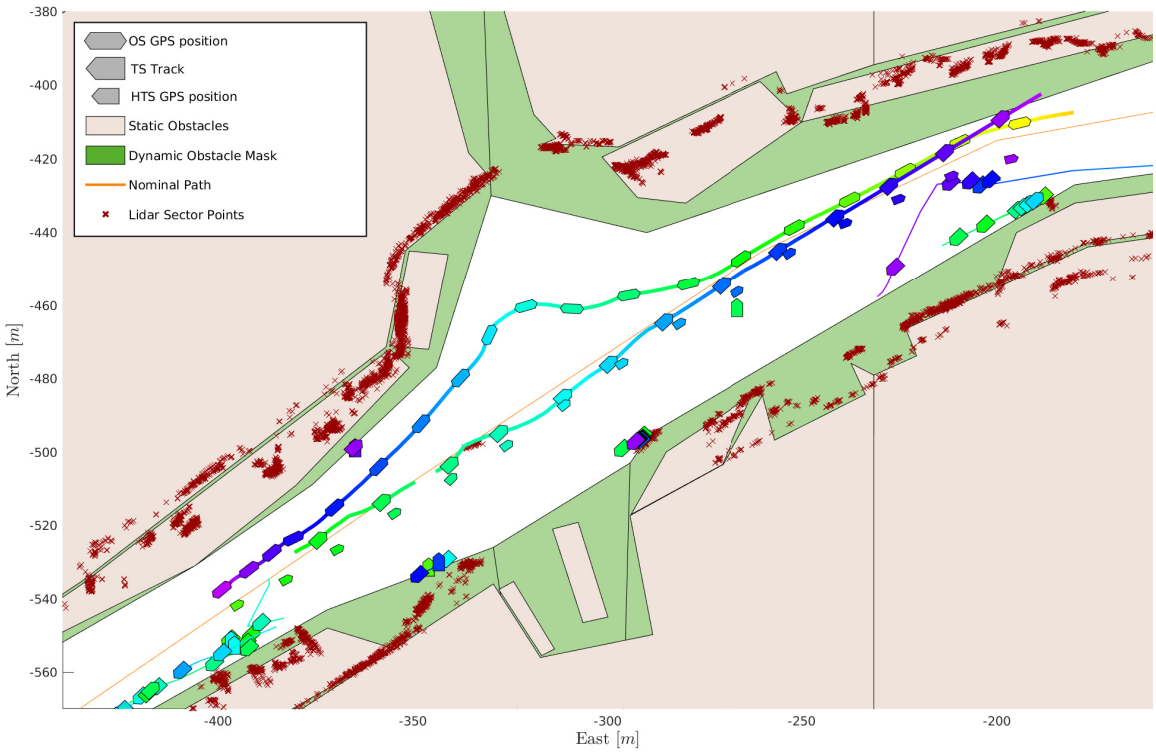

Figure 21. Experiment 1.1: The OS is traveling east to west, and performs a starboard maneuver to give way to the HTS. The HTS does not abide its give-way duty.

8.1.2. Head-on: Experiment 1.2

In this encounter, the OS is traveling west to east, and the HTS is traveling in the opposite direction. An overview of the experiment is shown in Figure 22. The detection of the HTS is somewhat late, yet at sufficient distance for the OS to perform an early and smooth starboard maneuver and pass port to port with the HTS in accordance with Rule 14. The magnitude of the starboard maneuver is small due to the course of the HTS, which is also on a small starboard maneuver. The two vessels pass each other at a safe distance, both between vessels and from vessels to static obstacles, and share the available space in the canal between them in a similar way as would be expected in an encounter by two manned vessels of equal size. This indicates that the algorithm is not only rules-compliant, but it produces behavior that is suitable for maneuvering among other manned vessels. The OS trajectory is unaffected by the false track detected to its starboard side close to the end of the transit, as this track is estimated to have zero velocity.

8.1.3. Head-on: Experiment 1.3

The OS is traveling east to west, opposite to the HTS, as can be seen by the experiment overview in Figure 23. The overview shows that several false tracks were detected, yet most of them were not in proximity to the OS. However, one track close to $[N, E] = [-450, -240]$ existing for only a few seconds caused the OS to start a starboard maneuver, which is continued until the HTS is past and clear. Since the estimated position of the HTS as CPA is close to the center of the widest part of the canal, the size of the TS domain of the HTS is dimensioned based on the available maneuverable space to the port of the HTS at this point, making it larger than what is representative for the canal as a whole. This, in turn, results in a larger than necessary starboard maneuver, putting the OS in conflict with the static obstacles further down the canal, and causing it to maneuver back towards the path with a higher effort than desired, similar to what happened in Experiment 1.1.

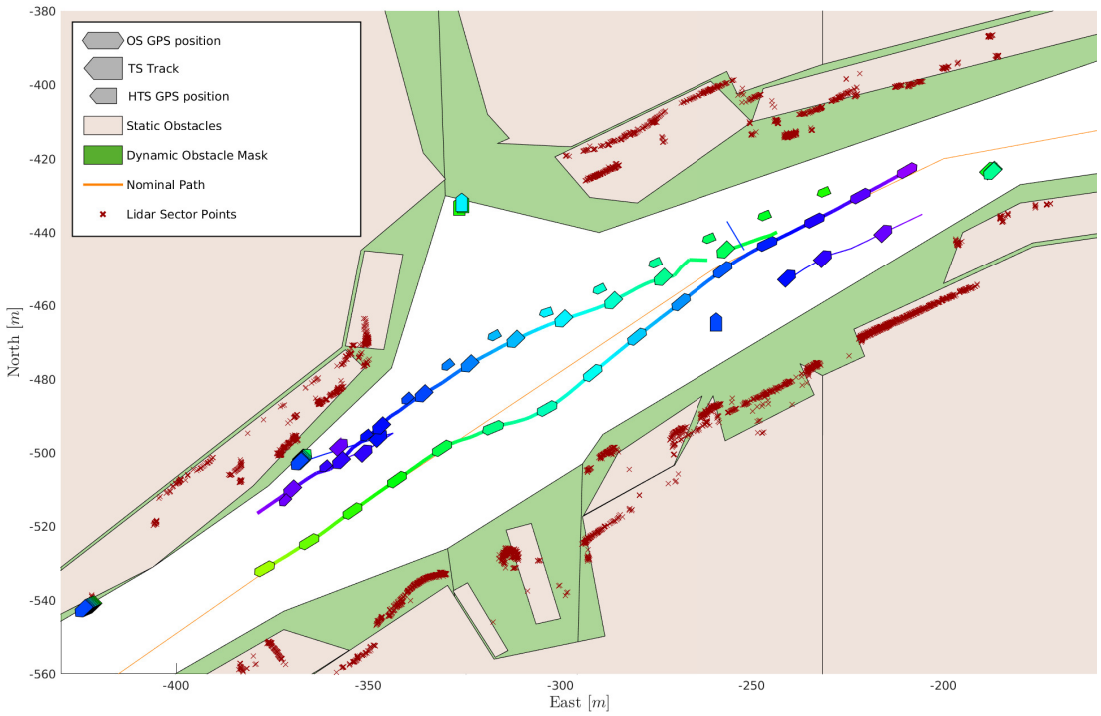

Figure 22. Experiment 1.2: The OS is traveling west to east, and performs a starboard maneuver to give way to the HTS. The starboard maneuver is small, but sufficient due to the course of the HTS.

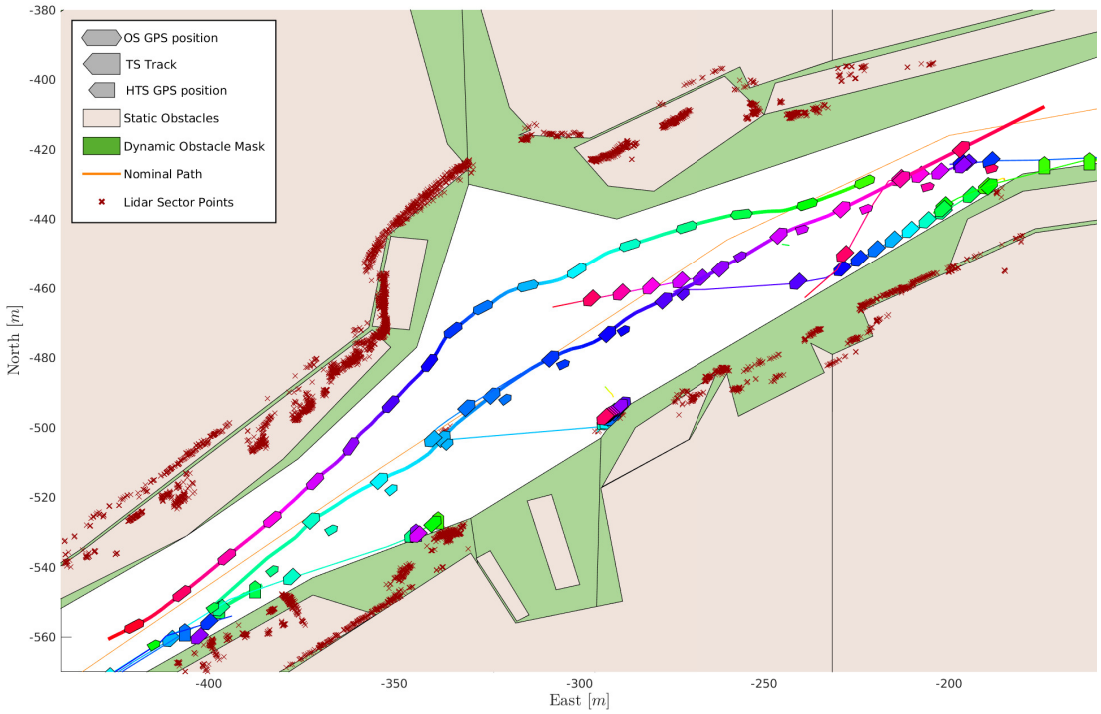

Figure 23. Experiment 1.3: The OS is traveling east to west. The starboard maneuver is initiated by a false track. The OS holds its starboard side of the canal until it is past and clear of the HTS.

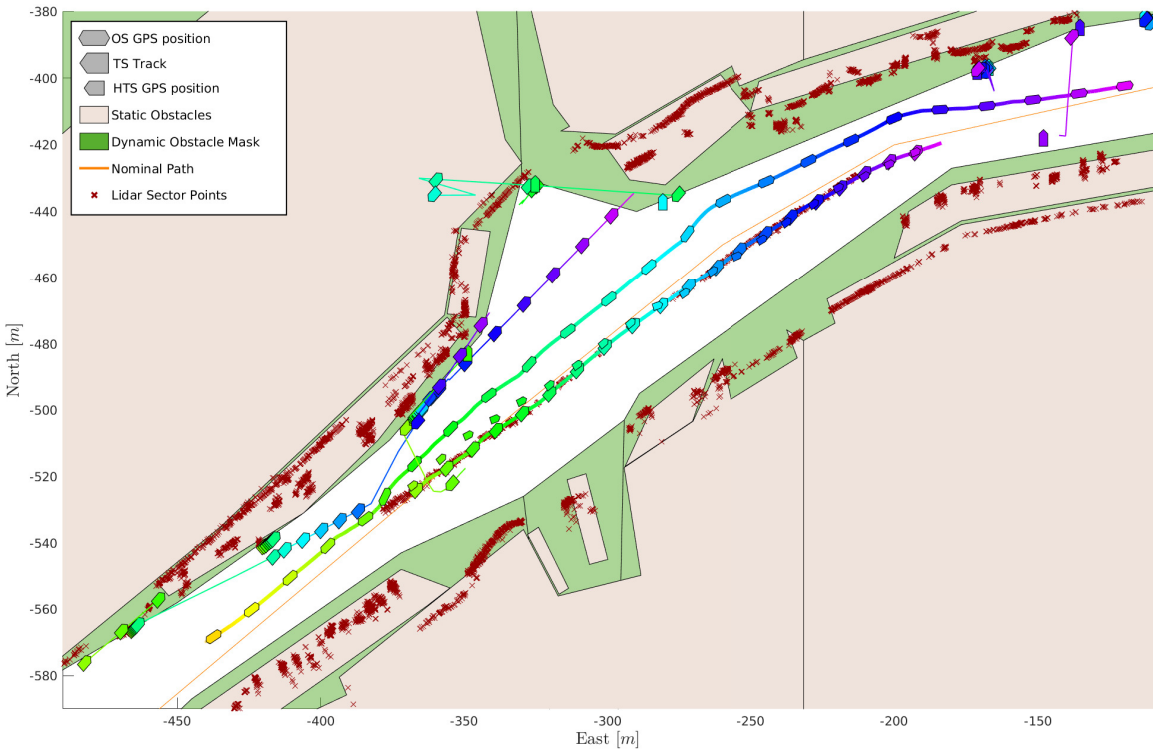

Figure 24. Experiment 2.1: The OS is traveling west to east and overtakes the HTS on its port side. The OS keeps to its port side of the canal until it is past and clear in front of the HTS.

8.1.4. Overtaking: Experiment 2.1

In this experiment, visualized in Figure 24, both the OS and the HTS are traveling west to east, where the OS starts off behind the HTS. The encounter is classified as an overtaking encounter, and the OS maneuvers to the port to pass the HTS on its port side. Due to the small relative velocity between the vessels, the overtaking maneuver lasts for more than 200 m through the canal. Yet, the OS keeps a safe distance to the HTS throughout the maneuver, and only moves back onto its path when it is finally past and clear, in accordance with Rule 13.

8.1.5. Overtaking: Experiment 2.2

In this overtaking scenario, both the OS and the HTS are traveling east to west. An overview is given in Figure 25. The OS starts a maneuver to overtake the HTS on its port side and continues this maneuver throughout the scenario. Note how the OS moves closer to the HTS towards the end of the overtaking due to the reduced free space, yet still keeps a safe distance as a result of the considerations introduced in Section 4.2. Due to the low relative velocity between the OS and the HTS, the maneuver lasts so long that the OS travels out of the area of the mask for the dynamic obstacles. Towards the end of the transit, the OS reacts to several tracks that originate from the vessels docked along the canal. Several of the tracks also receive estimated velocities from movement of its center of mass due to clustering and declustering of several vessels, resulting in the OS performing a port maneuver due to an oncoming false track.

8.1.6. Crossing: Experiment 3.1

In this crossing scenario, the OS is crossing the canal from south to north, while the HTS is traveling east to west along the canal. The OS is initially on DP at the start of the nominal path, and the transit is initiated when the HTS is in a position that will result in an encounter. An overview of

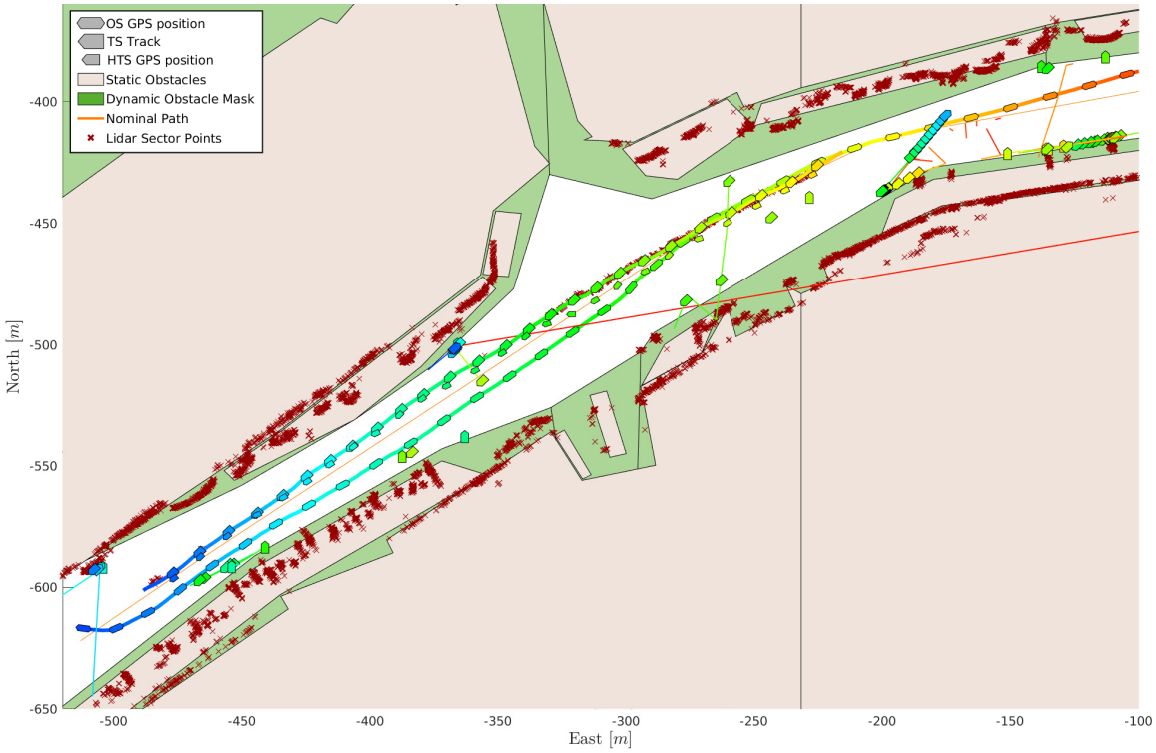

Figure 25. Experiment 2.2: The OS is traveling east to west, and overtakes the HTS in a long overtaking maneuver, where the available space is reduced towards the end. At the end of the maneuver, the OS performs a starboard maneuver due to a detected false track.

the scenario is given in Figure 26. The OS starts off with a starboard maneuver to pass behind the HTS, and it proceeds towards the destination waypoint once it is is clear behind the HTS.

8.1.7. Crossing: Experiment 3.2

In this scenario, the OS is crossing the canal from north to south, while the HTS is traveling west to east. An overview is given in Figure 27. The OS has give-way obligations, and it starts with a starboard maneuver to pass behind the HTS, and proceeds along the transit once it is passed and clear behind the HTS. The encounter is resolved without collision, and the OS acts in accordance with Rule 16.

8.1.8. Crossing: Experiment 3.3

In this crossing scenario, the OS is crossing the canal from south to north, while the HTS is traveling east to west along the canal. A scenario overview is given in Figure 28. The OS has give-way obligations, and it starts a starboard maneuver to pass behind the HTS. The maneuver is subsequently halted by the presence of a static obstacle detected by the lidar, as is apparent from the concentration of lidar sector points to the east of the OS in the scenario overview. In this scenario, the transit is started with the HTS further from the nominal path of the OS, compared to Experiment 3.1, which means the OS has to make a larger starboard maneuver in order to stay clear of the HTS domain while maintaining the reference speed. Additionally, since the conflicting static obstacle is missing from the map data, and is not taken into account when calculating the available maneuverable space and the size of the TS domain, the HTS TS domain is larger than the actual encounter would require. The combination of these factors results in a restricted safe set, and hence the OS has to wait for the HTS to pass before proceeding with the transit.

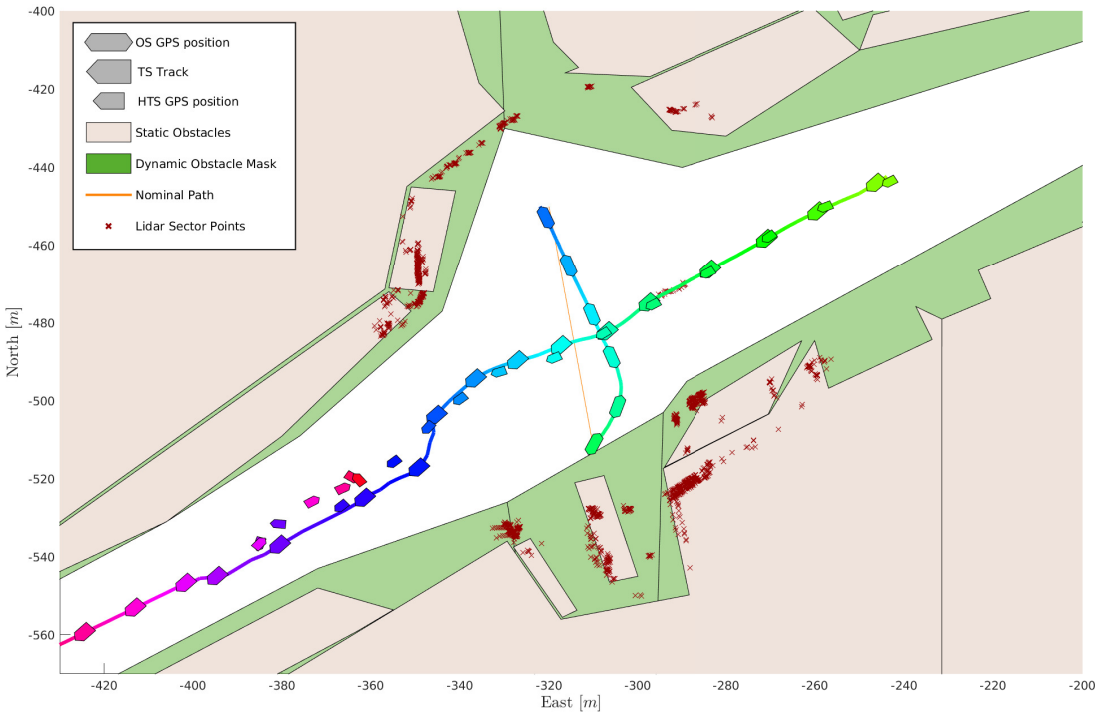

Figure 26. Experiment 3.1: The OS has give-way obligations in the crossing, and performs a starboard maneuver to pass behind the HTS.

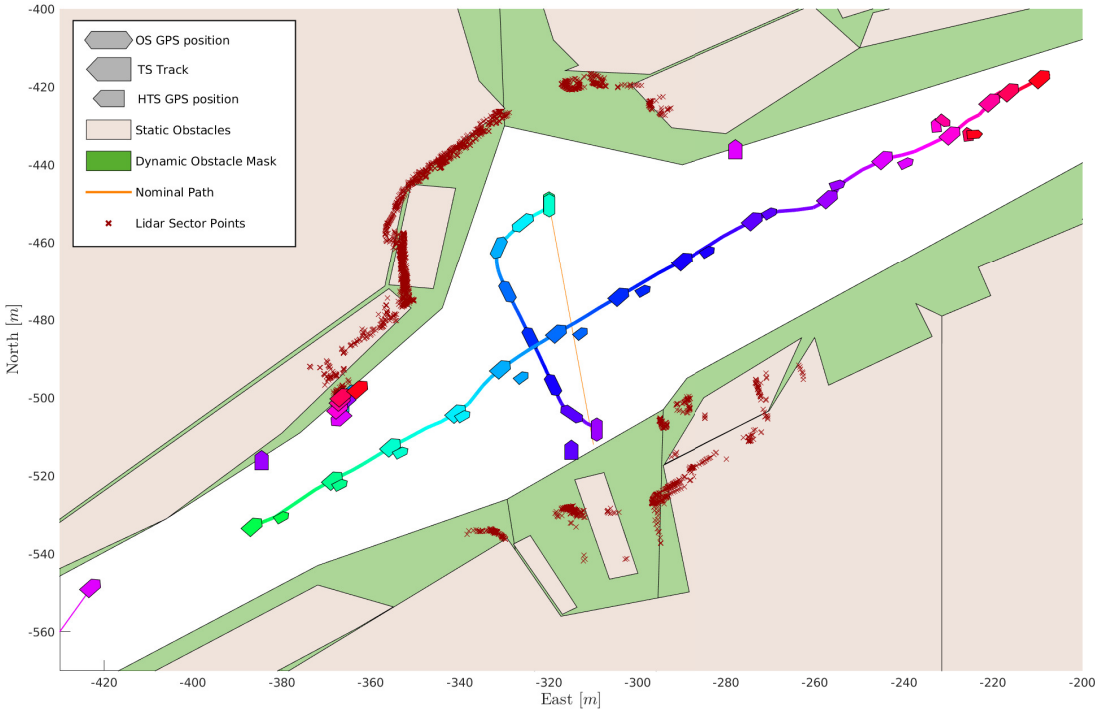

Figure 27. Experiment 3.2: The OS is traveling north to south and performs a starboard maneuver to cross behind the HTS.

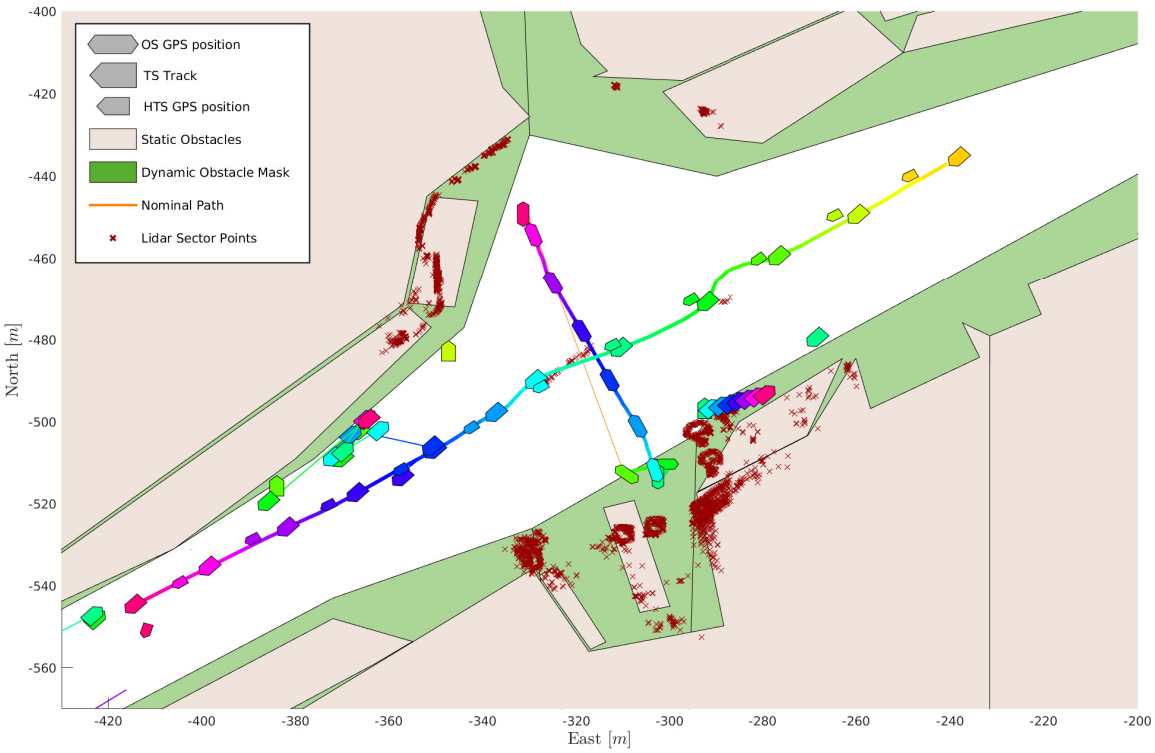

Figure 28. Experiment 3.3: The OS has give-way obligations to the HTS in the crossing encounter. An early starboard maneuver is halted by the presence of unmapped static obstacles detected by the lidar. The OS proceeds the transit when the HTS has passed.

8.1.9. Crossing: Experiment 3.4

In this scenario, the OS is traveling south to north, while the HTS is traveling west to east. It is therefore the HTS that has give-way obligations, while the OS is the stand-on vessel. An overview is given in Figure 29. Since the HTS is not abiding its give-way obligations, the OS performs a starboard maneuver to avoid collision and passes in front of the HTS. This encounter could also be resolved by a port maneuver by the OS. However, this would be in conflict with a rules-compliant starboard maneuver from the HTS, and it could, depending on the encounter geometry, involve a higher risk of collision. The threshold for maneuvering in front versus behind the TS in such encounters can be set through the classification-specific α_{δ_s} parameter.

8.2. Discussion

In several of the experiments, the position of the OS is outside the safe set $\mathcal{C}$ for longer periods. This is not obvious from the scenario plots presented in this paper, but it can be seen from the video animations of the experiments at this OneDrive **link**.[7] The violation may arise from one of two causes:

- A TS is detected with a position and velocity so that it immediately puts the OS in conflict with $\mathcal{C}$, or in such a way that it is inevitable that the OS will violate $\mathcal{C}$.
- The OS is initially in $\mathcal{C}$, but it does not apply the appropriate maneuvering effort to stay within $\mathcal{C}$ as the boundaries of the set change.

[7] Full link provided in earlier footnote

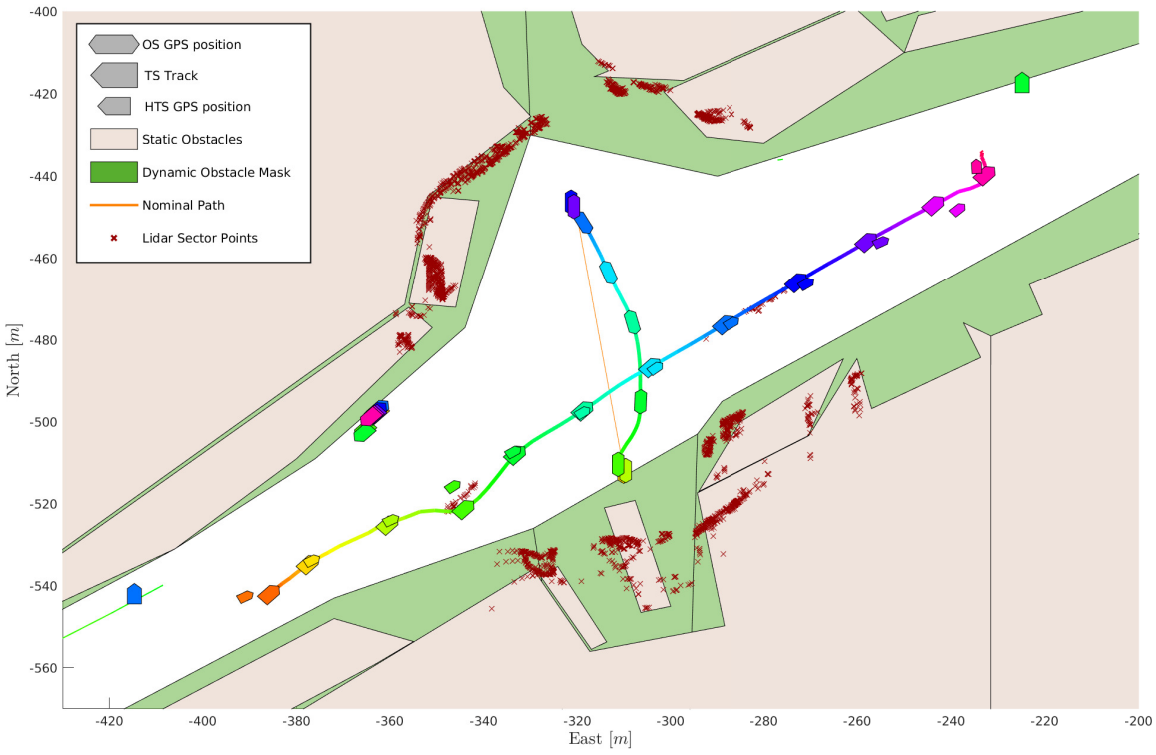

Figure 29. Experiment 3.4: The OS has stand-on obligations, but performs a starboard maneuver to stay clear of the HTS as the HTS fails to abide its give-way duty.

The first cause can be mitigated by improving the situational awareness modules, and in particular the target detection and tracking, by either improving algorithms or augmenting the perception system with additional sensors such as EO and IR cameras. The second cause arises from both modeling errors and state estimation errors on the models and state included in the CBF, in particular, estimates for $\boldsymbol{p}_{TS}$ and $\dot{\boldsymbol{p}}_{TS}$, and the exclusion of $\ddot{\alpha}$ in the dynamics of the TS domain. Additionally, any potential allocation error, the error between $\boldsymbol{\tau}$, and the resultant force produced by the thrusters are unaccounted for due to the absence of thruster dynamics in the vessel model. A way to mitigate this problem is to apply a hybrid CBF, where the c_{dyn} gain can be switched based on whether the corresponding domain is in violation or not. By reducing c_{dyn} once the domain is violated, the CBF constraint would require a higher velocity vector pointing out of the domain, and hence reduce the duration that the domain is in violation. Another approach is to apply robust CBFs to mitigate the effect of the uncertainties in the estimations, as proposed in (Cheng et al., 2020).

The proposed COLAV method favors course change maneuvers over speed change maneuvers, due to the dual objective of traversing along the path at transit speed while avoiding collision. Major speed adjustments are only made when traveling with a velocity component in the direction of the nominal path is made impossible by the presence of obstacles, as is the case in Experiment 3.3, where the OS moves in the opposite direction of the path at an early point in the transit. However, the COLREGs do dictate that "if there is sufficient sea-room," alteration of course alone is the preferred action. Furthermore, it is suggested that any alteration of course (or speed) should be of such magnitude that it is readily apparent to other vessels observing visually or by radar. For vessels operating in open waters, and observing each other at distances of several thousand meters, course change maneuvers of more than 60° are advised, as this will increase the chances of observing it by radar. However, for vessels moving in more confined spaces, and at much closer range, such maneuvering efforts might not be feasible, and they may not be necessary, as the proximity and

the presence of static obstacles make the maneuvers easier to comprehend. As an example, one can consider Experiment 1.2, where a small course change of about 15 degrees in the narrow canal is sufficient to demonstrate that the OS is maneuvering to its starboard side of the canal to give way for the approaching HTS. However, as can be seen from Figure 12, when there is sufficient room to maneuver, applying the proposed method does result in course-change maneuvers of much higher magnitude in encounters where the OS has give-way obligations.

In all the crossing scenarios, the OS resolves the encounter by maneuvering away from the nominal path to pass either in front of or behind the HTS. Even though the COLREGs favor course-change maneuvers over speed-change maneuvers, the maneuver increases the transit length considerably, and the maneuvering effort is large compared to reducing speed and waiting for the TS to pass before proceeding with the transit. This is a result of the reactive nature of the approach, where the OS reacts only to the current states, and it does not have any means for global optimization. This is mostly relevant for shorter transits, where the relative increase in trajectory length from course-change maneuvers is large. This issue can, however, be mitigated by applying the approach in a hybrid structure, with a long-term trajectory planner capable of adjusting the speed, such as the one in (Thyri et al., 2020b), which is designed specifically for short-transit operations.

From the lidar data in the overview figures, one can get an indication that there is a slowly varying bias in the position estimate of the OS. This is most apparent when comparing the lidar points on the south bank in the eastern part of the canal in Figures 21 and 24, where the lidar sector points are in the water in the first figure, and several meters inside the polygon representing the canal bank in the second figure. This navigation error is outside the limits of the RTK GPS precision, and it seems to arise from the GPS system failing to maintain a link with the RTK antenna during several of the experiments, and hence falling back on a standard GPS solution. Although the navigation bias can be compensated for by, for example, lidar-based SLAM algorithms, the risk of navigation errors and failure will always exist. This highlights the need for a COLAV method for static obstacles that is based on exteroceptive sensors, which provide obstacle position estimates relative to the position of the OS, hence the method would be unaffected by navigation errors.

Lastly, note the number of static obstacles that are detected in proximity to the OS during a transit, but are not represented in the map data. For example, the obstacle halting the transit in Figure 28 is actually two thick wooden poles tied together with a sign on the top. In addition, the object to the southwest in Figure 22, which has the shape of the hull of a boat, is actually the hull of a boat, as can be seen from the drone footage in Figure 1 taken from the north side of the canal. These objects effectively occupy relatively large parts of the free space from the map data, which again highlights the importance of a reactive COLAV module based on exteroceptive sensors. However, for a more robust solution, the map for static obstacles should be continuously updated, based on new sensor data, to include unmapped static features such as sea markings, poles, and harbors, and temporarily or quasistatic features such as docked vessels and floating harbors. By applying such an approach, superior estimates of r_{free} can be made.

9. Conclusion and future work

A domain-based reactive COLAV method has been presented, where the method is made compliant with COLREGs Rules 13–15 and 17 through a novel target ship (TS) domain design. The TS domain is parametrized by a few rule-based parameters, and the domain size is adaptive and based on the available space to maneuver around the TS at CPA. The rule-based parameters of the TS domains are determined by a COLREGs-based classification of each vessel-to-vessel encounter, where we propose improvements to an existing encounter classification method. Violation of the TS domains and domains for static obstacles is avoided by formulating control barrier functions for each domain.

The effectiveness of the TS domain is demonstrated through an extensive set of simulations of V2V encounters where the TS keeps a constant course and speed. The proposed COLAV method produces both protocol compliant and well-behaved trajectories for a vast majority of the simulations, and it avoids collision in a compliant manner in all simulations. The method is also demonstrated through

simulation of complex scenarios, with multiple autonomous vessels operating in a confined area. In these simulations, the method proves to be robust, where the adaptive domain size effectively distributes the available space between the vessels to ensure safe conduct.

Lastly, the method is demonstrated through several full-scale experiments in a relevant environment with a controlled TS. In the experiments, a target tracker based on radar and lidar is applied for estimating the position and velocity of target ships. Additionally, lidar is used to compensate for uncertainty in map data for COLAV w.r.t. static obstacles. The proposed method shows good performance in combination with a realistic target tracking system, and it handles all encounters in a COLREGs-compliant manner. By including lidar for COLAV w.r.t. static obstacles, risks associated with unmapped obstacles and uncertainties in map data, navigation, and target tracking can be mitigated, and the baseline safety of the method can be ensured.

Future work includes:

- Applying the TS domain to a model predictive controller in a deliberate midlevel COLAV module, to improve performance w.r.t. Rule 8 regarding early action, and also to reduce the effect of the stagnation points of the TS domain, and improve the tradeoff between course change maneuvers and speed change maneuvers.
- More extensive simulation-based verification of the method in multivessel encounters.
- Further work on the encounter classification through improved intent inference.
- Pairing the proposed reactive COLAV method with a deliberate planner that considers a complementing subset of the COLREGs, in particular trajectory planning w.r.t. local traffic regulations, and adapting the velocity to ensure safe conduct when vessels are approaching in confined waters.

Acknowledgments

This work was supported by the NTNU Digital transformation project Autoferry and the Research Council of Norway through the Centres of Excellence funding scheme, project no. 223254. The authors would like to thank Erik Wilthil for his contribution to the experiments, both as crew member on the milliAmpere, and for providing the target tracker.

ORCID

Emil Hjelseth Thyri https://orcid.org/0000-0002-7635-8055
Morten Breivik https://orcid.org/0000-0002-0457-1850

References

Ames, A. D., Coogan, S., Egerstedt, M., Notomista, G., Sreenath, K., and Tabuada, P. (2019). Control barrier functions: Theory and applications. In *Proceedings of the 2019 18th European Control Conference (ECC)*, pages 3420–3431, Naples, Italy.

Atallah, M. J., Ribeiro, C. C., and Lifschitz, S. (1991). Computing some distance functions between polygons. *Pattern Recognition*, 24(8):775–781.

Basso, E. A., Thyri, E. H., Pettersen, K. Y., Breivik, M., and Skjetne, R. (2020). Safety-critical control of autonomous surface vehicles in the presence of ocean currents. In *Proceedings of the 2020 4th IEEE Conference on Control Technology and Applications (CCTA)*, pages 396–403, Montreal, Canada.

Benjamin, M. R., Leonard, J. J., and Newman, P. M. (2006). A method for protocol-based collision avoidance between autonomous marine surface craft. *Journal of Field Robotics*, 25(5):333–346.

Blenkey, N. (2021). Kongsberg gets EU funding to demo two autonomous vessels. *Marine Log*.

Cairns, R. (2021). Norway pioneered electric ferries. Now it's making them self-driving. *CNN Travel*.

Cheng, R., Khojasteh, M. J., Ames, A. D., and Burdick, J. W. (2020). Safe multi-agent interaction through robust control barrier functions with learned uncertainties. In *Proceedings of the 2020 59th IEEE Conference on Decision and Control (CDC)*, pages 777–783, Jeju Island, Republic of Korea.

Cockcroft, A. N. and Lameijer, J. N. F. (2012). *Guide to the Collision Avoidance Rules.* Butterworth-Heinemann.

Eriksen, B.-O. H., Bitar, G., Breivik, M., and Lekkas, A. M. (2020). Hybrid collision avoidance for ASVs compliant with COLREGs rules 8 and 13–17. *Frontiers in Robotics and AI*, 7:11.

Eriksen, B.-O. H. and Breivik, M. (2019). Short-term ASV collision avoidance with static and moving obstacles. *Modeling, Identification and Control*, 40:177–187.

Eriksen, B.-O. H., Breivik, M., Wilthil, E., Flaten, A., and Brekke, E. (2019). The branching-course model predictive control algorithm for maritime collision avoidance. *Journal of Field Robotics*, 36:1222–1249.

Fossen, T. I. (2011). *Handbook of Marine Craft Hydrodynamics and Motion Control.* John Wiley & Sons.

Goodwin, E. M. (1975). A statistical study of ship domains. *Journal of Navigation*, 28(3):328–344.

Huang, Y., Chen, L., Chen, P., Negenborn, R. R., and van Gelder, P. (2020). Ship collision avoidance methods: State-of-the-art. *Safety Science*, 121:451–473.

Kartverket (2020). Kartkatalogen. *https://kartkatalog.geonorge.no/.*

Kufoalor, D. K. M., Wilthil, E., Hagen, I. B., Brekke, E. F., and Johansen, T. A. (2019). Autonomous COLREGs-compliant decision making using maritime radar tracking and model predictive control. In *Proceedings of the 2019 18th European Control Conference (ECC)*, pages 2536–2542, Naples, Italy.

Kuwata, Y., Wolf, M. T., Zarzhitsky, D., and Huntsberger, T. L. (2014). Safe maritime autonomous navigation with COLREGs, using velocity obstacles. *IEEE Journal of Oceanic Engineering*, 39(1):110–119.

Loe, Ø. A. G. (2008). Collision avoidance for unmanned surface vehicles. Master's thesis, Norwegian University of Science and Technology, Trondheim, Norway.

Martinsen, A. B., Bitar, G., Lekkas, A. M., and Gros, S. (2020). Optimization-based automatic docking and berthing of ASVs using exteroceptive sensors: Theory and experiments. *IEEE Access*, 8:204974–204986.

O'Dwyer, R. (2021). ASKO to build two autonomous vessels for Oslo fjord operations. *Smart Maritime Network*.

Pedersen, A. A. (2019). Optimization based system identification for the milliAmpere ferry. Master's thesis, Norwegian University of Science and Technology (NTNU), Trondheim, Norway.

Schuster, M., Blaich, M., and Reuter, J. (2014). Collision avoidance for vessels using a low-cost radar sensor. *IFAC Proceedings Volumes*, 47(3):9673–9678. 19th IFAC World Congress.

Shah, B. C., Svec, P., Bertaska, I. R., Sinisterra, A. J., Klinger, W., von Ellenrieder, K., Dhanak, M., and Gupta, S. K. (2016). Resolution-adaptive risk-aware trajectory planning for surface vehicles operating in congested civilian traffic. *Autonomous Robots*, 40:1139–1163.

Stensvold, T. (2020). Trondheim første by med autonom passasjertransport på vannet - Oslo kan bli neste. *Teknisk Ukeblad*.

Svec, P., Shah, B. C., Bertaska, I. R., Alvarez, J., Sinisterra, A. J., von Ellenrieder, K., Dhanak, M., and Gupta, S. K. (2013). Dynamics-aware target following for an autonomous surface vehicle operating under COLREGs in civilian traffic. In *Proceedings of the 2013 IEEE/RSJ International Conference on Intelligent Robots and Systems*, pages 3871–3878.

Tam, C. and Bucknall, R. (2010). Collision risk assessment for ships. *Journal of Marine Science and Technology*, 15:257–270.

Thyri, E. H., Basso, E. A., Breivik, M., Pettersen, K. Y., Skjetne, R., and Lekkas, A. M. (2020a). Reactive collision avoidance for ASVs based on control barrier functions. In *Proceedings of the 2020 4th IEEE Conference on Control Technology and Applications (CCTA)*, pages 380–387, Montreal, QC, Canada.

Thyri, E. H., Breivik, M., and Lekkas, A. M. (2020b). A path-velocity decomposition approach to collision avoidance for autonomous passenger ferries in confined waters. In *Proceedings of the 20th IFAC World Congress*, pages 14628–14635, Berlin, Germany.

Torben, T. R., Brodtkorb, A. H., and Sørensen, A. J. (2019). Control allocation for double-ended ferries with full-scale experimental results. *IFAC-PapersOnLine*, 52(21):45–50. 12th IFAC Conference on Control Applications in Marine Systems, Robotics, and Vehicles (CAMS), Daejeon, South Korea.

Vagale, A., Bye, R. T., Oucheikh, R., Osen, O. L., and Fossen, T. (2021a). Path planning and collision avoidance for autonomous surface vehicles II: A comparative study of algorithms. *Journal of Marine Science and Technology*, pages 1–17.

Vagale, A., Oucheikh, R., Bye, R., Osen, O., and Fossen, T. (2021b). Path planning and collision avoidance for autonomous surface vehicles I: A review. *Journal of Marine Science and Technology*, pages 1–15.

Wilthil, E. F., Brekke, E., and Asplin, O. B. (2018). Track initiation for maritime radar tracking with and without prior information. In *Proceedings of the 2018 21st International Conference on Information Fusion (FUSION)*, pages 1–8, Cambridge, UK.

Wilthil, E. F., Flåten, A. L., and Brekke, E. F. (2017). *A Target Tracking System for ASV Collision Avoidance Based on the PDAF*, pages 269–288. Springer International Publishing.

Woerner, K. (2016). *Multi-Contact Protocol-Constrained Collision Avoidance for Autonomous Marine Vehicles*. PhD thesis, Massachusetts Institute of Technology.

How to cite this article: Thyri E. H., & Breivik M. (2022). A domain-based and reactive COLAV method with a partially COLREGs-compliant domain for ASVs operating in confined waters. *Field Robotics, 2*, 637–677.